The forced response of the El Niño–Southern Oscillation-Indian monsoon teleconnection in ensembles of Earth System Models

The forced response of the El Niño–Southern Oscillation-Indian monsoon teleconnection in ensembles of Earth System Models

Tamás Bódai[1,2,3,4], Gábor Drótos[5,6,7], Mátyás Herein[6,8,*], Frank Lunkeit[8], Valerio Lucarini[3,4,8,9]

[1]Pusan National University, Busan, Republic of Korea

[2]Center for Climate Physics, Institute for Basic Science, Busan, Republic of Korea

[3]Department of Mathematics and Statistics, University of Reading, Reading, UK

[4]Centre for the Mathematics of the Planet Earth, University of Reading, Reading, UK

[5]Instituto de Física Interdisciplinar y Sistemas Complejos, CSIC-UIB, Palma de Mallorca, Spain

[6]MTA–ELTE Theoretical Physics Research Group, and Institute for Theoretical Physics, Eötvös University, Budapest, Hungary

[7]Max-Planck-Institut für Meteorologie, Hamburg, Germany

[8]CEN, Meteorological Institute, University of Hamburg, Hamburg, Germany

[9]Walker Institute for Climate System Research, University of Reading, Reading, UK

*hereinm@gmail.com

Abstract

We study the teleconnection between the El Niño–Southern Oscillation (ENSO) and the Indian summer monsoon (IM) in large ensemble simulations, the Max Planck Institute Earth System Model (MPI-ESM) and the Community Earth System Model (CESM1). We characterize ENSO by the JJA Niño 3 box-average SST and the IM by the JJAS average

Early Online Release: This preliminary version has been accepted for publication in *Journal of Climate*, may be fully cited, and has been assigned DOI 10.1175/JCLI-D-19-0341.1. The final typeset copyedited article will replace the EOR at the above DOI when it is published.

precipitation over India, and define their teleconnection in a changing climate as an ensemble-wise correlation. To test robustness, we also consider somewhat different variables that can characterize ENSO and the IM. We utilize ensembles converged to the system's snapshot attractor for analyzing possible *changes in the teleconnection*. Our main finding is that the teleconnection strength is typically increasing on the long term in view of appropriately revised ensemble-wise indices. Indices involving a more western part of the Pacific reveal, furthermore, a short-term but rather strong increase in strength followed by some decrease at the turn of the century. Using the station-based SOI as opposed to area-based indices leads to the identification of somewhat more erratic trends, but the turn-of-the-century "bump" is well-detectable with it. All this is in contrast, if not in contradiction, with the discussion in the literature of a weakening teleconnection in the late 20th century. We show here that this discrepancy can be due to any of three reasons: ensemble-wise and temporal correlation coefficients used in the literature are different quantities; the temporal moving correlation has a high statistical variability but possibly also persistence; MPI-ESM does not represent the Earth system faithfully.

1. Introduction

Probably the most important teleconnection phenomena are those of the El Niño–Southern Oscillation (ENSO) (Trenberth, 1976; Trenberth, 1984; Bjerknes, 1969; Neelin, 1998). ENSO is a natural, irregular fluctuation phenomenon in the tropical Pacific region (Timmermann et al., 2018), and mostly affects the tropical and the subtropical regions; however, it has an impact on the global climate system as well. A crucial and open question that has challenged scientists for decades is how ENSO would change as a result of the increasing radiative forcing due to the increasing greenhouse gas concentrations. The IPCC has low confidence in

Accepted for publication in *Journal of Climate*. DOI 10.1175/JCLI-D-19-0341.1.

what would exactly happen to ENSO in the future, even though they have high confidence that ENSO itself would continue (Christensen et al., 2013). There have been several studies (e.g. Guilyardi et al., 2009; Collins et al., 2010; Vecchi and Wittenberg, 2010; Cai et al., 2015) that aimed to reveal how ENSO might respond to greenhouse-gas forcing. However, most of the applied methods have a common drawback: they evalute averages and further statistical quantifiers (including variances, correlations, etc.) with respect to time in a time-dependent dynamical system, i.e., in our changing climate, or in simplified models thereof.

In a changing climate, where one or more relevant parameters are changing in time, there can be no stationarity by definition, whereas stationarity is crucial for the applicability of temporal averages, as illustrated by Drótos et al. (2015) in a toy model. In realistic GCMs globally averaged quantities seem to behave better, but the problem proves to be significant for local quantities and teleconnections (Herein et al., 2016, Herein et al., 2017). Since the ENSO events are identified by temperatures that are warmer or cooler than average, and teleconnections are defined as correlations between such anomalies, it is important to have a firmly established notion of averages when climatic means are shifting, as also pointed out by L'Heureux et al. (2013, 2017) and Lindsey et al. (2013).

To properly address the problem of evaluating averages in a changing climate, in this study we turn to a gradually strengthening view according to which the relevant quantities of the climate system are the statistics taken over an ensemble of possible realizations evolved from various initial conditions (see e.g. Bódai et al., 2011; Bódai and Tél, 2012; Deser et al., 2012; Daron and Stainforth, 2015; Kay et al., 2015; Stevens, 2015; Bittner et al., 2016; Herein et al., 2016; Herein et al., 2017; Drótos et al., 2017; Hedemann et al., 2017; Lucarini et al., 2017; Suárez-Gutiérrez et al., 2017; Li et al., 2018; Maher, 2019). We can trace back this view to

Accepted for publication in *Journal of Climate*. DOI 10.1175/JCLI-D-19-0341.1.

Leith (1978), which was recently revived (Branstator & Teng 2010) and rediscovered independently also by others. In contrast to weather forecast, one focuses here on long-term properties, independent of initial conditions, in order to characterize the internal variability, as well as the forced response of the climate. The mathematical concept that provides an appropriate framework is that of snapshot (Romeiras et al., 1990; Drótos et al., 2015) or pullback attractors (Arnold, 1998; Ghil et al., 2008; Chekroun et al., 2011); and the concept's applicability has also been demonstrated in laboratory experiments (Vincze et al., 2017) as well as to tipping dynamics (Kaszás, 2019).

Qualitatively speaking, a snapshot attractor is a unique object in the phase space of dissipative systems with arbitrary, non-periodic forcing, to which an ensemble of trajectories converges within a basin of attraction. In the climatic context, the ensemble members can be regarded as Earth systems evolving in *parallel*, all of which are controlled by the *same* physics and are subject to the *same* external forcing (Leith 1978; Herein et al., 2017). If the dynamics is chaotic, convergence implies that the initial condition of the ensemble is "forgotten": after some time (the convergence time) the evolution of the particular ensemble becomes independent of how it was initialized; instead, the distribution of its members, at any time instant, becomes determined by the natural probability distribution of the attractor. This means that the ensemble members, in the given time instant, characterize the plethora of all possible weather situations permitted in the Earth system in a probabilistically correct way (Drótos et al., 2017). The snapshot attractor and its natural distribution depend on time in general, and *their time evolution is determined uniquely by the forcing* scenario of the system. Note that ensemble statistics are instantaneous by construction.

Accepted for publication in *Journal of Climate*. DOI 10.1175/JCLI-D-19-0341.1.

In this paper we directly construct the snapshot attractor and its natural probability distribution, following Herein et al. (2017) (see also Sec. 4), and apply our methodology – foreseen already by Leith (1978) – to the teleconnection of ENSO and the Indian summer monsoon. To our knowledge, it is the first time that the snapshot approach (taking care of the convergence) is used in the context of the ENSO-Indian monsoon teleconnection. Although an externally forced system is almost surely nonstationary, in a finite ensemble this signal might not show up. Here we will resort to statistical tests against the null-hypothesis of stationarity in order to "detect nonstationarity" and learn about its nature.

2. Subjects of the study

Our investigations concern ensemble simulations from two state-of-the-art climate models: the Community Earth System Model (CESM, Hurrell et al. (2012)) and the Max Planck Institute Earth System Model (MPI-ESM, Giorgetta et al. (2013)).

The CMIP5 versions of these models were already studied regarding how reliable their ENSO characteristics are. It is known that both models underestimate the ENSO asymmetry, but all of the CMIP5 models suffer from this problem (Zhang and Sun, 2014). Generally, however, both models show relatively good ENSO characteristics compared to observations (Bellenger et al., 2014; Capotondi, 2013). The pattern of the monsoon precipitation is quite realistic in both models (see also our analysis in Sec. 6.1), however, the future projections for the Indian

Accepted for publication in *Journal of Climate*. DOI 10.1175/JCLI-D-19-0341.1.

region generally have a moderate confidence (Freychet et al., 2015). In the recent study of Ramu et al. (2018), the strength of the ENSO–IM teleconnection has been found to be considerably underestimated in both models compared to observations. We must note, however, that Ramu et al. (2018) calculate the correlation coefficient with respect to time in a historically forced single run, so that the resulting values are possibly unreliable, cf. Section 6.1.

We consider five ensembles in total. The CESM community designed the CESM Large Ensemble ('CESM-LE') with the explicit goal of enabling assessment of climate change in the presence of internal climate variability (Kay et al., 2015). All realizations use a single model version (CESM with the Community Atmosphere Model, version 5) at a resolution of 192 × 288 in latitudinal and longitudinal directions, with 30 atmospheric levels. The MPI-ESM (Giorgetta et al., 2013) was also used to produce ensembles (called together the 'Grand Ensemble', 'MPI-GE') to explore internal variability in a changing climate (Stevens, 2015; Bittner et al., 2016; Maher et al. 2019). The single configuration applied to this purpose is model version MPI-ESM1.1 in low-resolution (LR) mode, which corresponds to a horizontal resolution of T63 with 47 vertical levels in the atmosphere, and to 1.5-degree horizontal resolution with 40 vertical levels in the ocean.

The CESM Large Ensemble ('CESM-LE') consists of 35 comparable members and covers the time span of 1920-2100. Between 1920 and 2005, historical climate forcing (Lamarque et al., 2010) is used, and the RCP8.5 (van Vuuren et al., 2011) is applied afterwards, reaching a nominal radiative forcing of Q = 8.3 W/m^2 by 2100. The MPI-ESM historical ensemble ('MPI-HE' in what follows) has 63 members unaffected by spin-up artifacts in the ocean (Maher et al., 2019), and runs from 1850 to 2005 under historical climate forcing (Lamarque

Accepted for publication in *Journal of Climate*. DOI 10.1175/JCLI-D-19-0341.1.

et al., 2010). The nominal radiative forcing becomes thus $Q = 2.1$ W/m^2 by 2005 (similarly as in the CESM-LE). The MPI-ESM RCP2.6 and RCP8.5 ensembles (which we shall call 'MPI-RCP2.6E' and 'MPI-RCP8.5E') continue the previous runs between 2006 and 2099 under the RCP2.6 and the RCP8.5, respectively (van Vuuren et al., 2011): the former provides information about the effects of a pathway peaking in the early 21st century, while the latter assumes further growth in the anthropogenic emission. Finally, the MPI-ESM one-percent ensemble ('MPI-1pctE' in what follows), having 43 members of reliable output, starts in 1850 with the same (pre-industrial-like) external conditions as the MPI-HE. Being an idealized experiment, the CO_2 concentration is increased in this case by 1 percent per year until 1999, while the concentrations of other greenhouse gases and radiative agents are kept constant. The nominal radiative forcing (calculated via the logarithmic response (Ramaswamy et al., 2001)) reached by 1999 is $Q = 8.3$ W/m^2.

Fig. 1 gives an overview (Meinshausen et al., 2011) of the forcing scenarios, interpreted in terms of the nominal radiative forcing Q, in the time spans of our particular investigations (beginning in 1890, see later). Note that the nominal radiative forcing Q is *not* a parameter of the system, so that its time dependence is *not* a forcing from a dynamical point of view. Instead, we treat it as a proxy for the aggregated effect of all different forcing agents (which include different tracers in the atmosphere, as well as the varying solar activity and land use — except for the MPI-1pctE).

In order to ensure memory loss (i.e., convergence to the snapshot attractor (Drótos et al., 2015; Herein et al., 2016; Drótos et al., 2017)), in most cases we discard the first 40 years of the simulations (the only exceptions are the simulations forced by the RCP scenarios, which are continuations of the historical simulation). We emphasize that, in principle, a detailed and

Accepted for publication in *Journal of Climate*. DOI 10.1175/JCLI-D-19-0341.1.

dedicated investigation should be carried out in both models to determine the time scale of the convergence, as advocated in Drótos et al. (2017). Due to technical limitations, however, this is far beyond the scope of the present study, which we believe to nevertheless provide with reliable results with the assumption of maximum 40 years for the convergence time, see Part I of the Supplementary Material.

We note that our estimates for the convergence time correspond to the convergence properties that are determined by the atmosphere and the upper ocean with timescales of a few decades, and *not* those that characterize the deep ocean and its abyssal circulation, which has time scales of thousands of years. According to this time-scale separation, we conjecture that the adjustment of the slow climate variables corresponding to the abyssal circulation does not influence substantially the statistical properties investigated here. Note that, otherwise, all the studies on the 21st-century climate change performed by looking at the properties of an ensemble of simulations would be hopeless. The details of this time-scale separation in the climate system and its particular implications remain the topic of future research.

3. Characterizing ENSO in a changing climate

The phases of ENSO are traditionally characterized by looking at carefully constructed climate indices, which surrogate the dominant features of the behavior of the fields of interest of the climate system. Most directly – and commonly – the sea surface temperature (SST) is considered to characterize ENSO, which is given rise in part by oceanic Kelvin waves closely confined to the Equator (Dijkstra 2005). Indices of ENSO, the so-called Niño indices (Trenberth, 1997), are defined as the average SST in various rectangular regions stretched along the Equator, minus the temporal mean of that, then divided by its temporal standard

Accepted for publication in *Journal of Climate*. DOI 10.1175/JCLI-D-19-0341.1.

198 deviation, but traditionally involving some smoothing as well. Thereby, anomalously high and
199 low values of the Niño index are considered as “episodes” or phases of the fluctuation
200 phenomenon, called El Niño and La Niña, respectively (Trenberth 1997). Here we are not
201 concerned with episodes, nevertheless, we will naturally end up with using anomalies in our
202 context (Sec. 4).
203
204 What we need to decide about is the Equatorial Pacific *region* of interest. We choose the box
205 [5°N-5°S, 150°W-90°W] which defines the Niño 3 index, that is, we consider the average
206 SST, T_{N3}, in this box. This is so because we wish to check the consistency of our findings in
207 the ESM with a previous report on observational data analysis (Krishna Kumar et al. 1999)
208 which considers the the Niño 3 index.
209
210 To demonstrate the robustness of the detected changes in the ENSO-IM teleconnection in the
211 MPI-ESM, or the lack of that, we also consider the difference, denoted by p_{diff}, between the
212 seasonal mean of the sea level pressure at Tahiti and at Darwin ($p_{diff} = p_{Tahiti} - p_{Darvin}$). The
213 difference p_{diff} is the basis of the Southern Oscillation Index (SOI) as defined by the Bureau of
214 Meteorology of the Australian Government, and measures the strength of the Walker
215 circulation. This version, not involving statistical preprocessing of the time series of the sea-
216 level pressure before taking their difference, is also called the Troup SOI. An anomalously
217 low (high) value of p_{diff}, and so that of the SOI, indicates an El Niño (La Niña) phase (Troup,
218 1965), and, therefore, the SOI (p_{diff}) is negatively correlated with the Niño 3 (T_{N3}).
219
220 In the Supplementary Material (Part II), we recall from Herein et al. (2017) that climate
221 indices should be treated carefully in a changing climate. In particular, long-term temporal
222 averaging has to be avoided in their definition, and should be replaced by averaging with

Accepted for publication in *Journal of Climate*. DOI 10.1175/JCLI-D-19-0341.1.

respect to the ensemble (after convergence has occurred). In the following whenever we mention Niño 3 or SOI, we mean the revised ensemble-wise index/anomaly when needed: we subtract the ensemble mean from the quantity in question, and divide the result by the ensemble standard deviation. Indices or any anomalies defined in this proper way do not carry information about temporal shifts in the climatic mean of the corresponding original quantities (like T_{N3} or p_{diff}). Therefore, investigations of shifts in climatic means have to be and can be carried out separately from those targeting the internal variability as represented by anomalies only. We do not investigate the shift of means here, but it can be found in (Herein et al., 2018) for a setting somewhat different from here.

4. The ENSO-IM teleconnection in a changing climate of the MPI-ESM: a forced response of internal variability

4.1 Conceptual considerations

A special aspect of internal variability is the presence of teleconnections: for certain variables characterizing geographically distant regions, anomalies with respect to their climatic mean do not occur independently in a statistical sense. As an example, in the case of ENSO, if T_{N3} (p_{diff}) is anomalously low (high) during the summer months, there is a good chance that the precipitation of the Indian monsoon is anomalously high, and vice-versa (Trenberth, 1997). Although, Roy et al. (2019) reports that the teleconnection strength can be very different when filtering for canonical, Modoki or mixed ENSO events. Note that we will primarily consider the JJA average of T_{N3} and p_{diff} and the JJAS (monsoon season) average of the precipitation P to conform to traditional definitions and because the truly instantaneous

Accepted for publication in *Journal of Climate*. DOI 10.1175/JCLI-D-19-0341.1.

247 quantities would have much lower correlation. We will nevertheless use exactly one data point
248 from each year, which is the time period within which these quantities are defined.
249
250 The simplest way to quantify the strength of the (tele-) connection between two given
251 variables is via Pearson's correlation coefficient *r* (Rogers and Nicewander, 1988). Note that
252 the correlation coefficient is obtained, by definition, as the average of the product of the
253 anomalies (as defined by subtracting the average and dividing by the standard deviation, cf.
254 the previous section) of the corresponding quantities. Consequently, a correlation coefficient
255 between anomalies is the same as that between the original quantities. Therefore, in our
256 context of the teleconnection we can speak interchangeably about T_{N3} and Niño 3, on the one
257 hand, and p_{diff} and SOI, on the other hand. We underline that Pearson's correlation coefficient
258 is limited to detect a linear correlation between the two quantities of interest; nonetheless, it is
259 useful for having a first order picture of the existing correlations in the fields.
260
261 In Herein et al. (2017) it has been demonstrated that the traditional evaluation of correlation
262 coefficients, carried out via averaging over time, provides with grossly incorrect results under
263 a changing climate. It is thus important to evaluate correlation coefficients with respect to the
264 ensemble: in nonautonomous systems with explicit time dependence the two operations are
265 not equivalent. As evaluation over the ensemble can be done at *any* "instant" of time (after
266 convergence), it also enables one to monitor the temporal evolution of the strength of the
267 teleconnection during a climate change. This temporal evolution is one aspect of the response
268 of internal variability to an external forcing. This is what we shall investigate in this Section
269 for the teleconnection between ENSO and the Indian monsoon.
270

Accepted for publication in *Journal of Climate*. DOI 10.1175/JCLI-D-19-0341.1.

In particular, we numerically evaluate the ensemble-based correlation coefficient between the "instantaneous" JJA averages of the SST (T_{N3}) – or the sea level pressure difference (p_{diff}) between (gridpoints closest to) Tahiti (17°31' S, 21°26' E) and Darwin (12°28' S, 130°50' E) – and the "instantaneous" JJAS seasonal average precipitation (P) over India (except for a few states in order to keep to the AISMR data set being our reference; see Fig. 1 of (Parthasarathy et al. 1994)); with the "option" of p_{diff} it reads as:

$$r = \frac{\langle p_{diff}\, P \rangle - \langle p_{diff} \rangle \langle P \rangle}{\sqrt{\left(\langle p_{diff}^2 \rangle - \langle p_{diff} \rangle^2\right)\left(\langle P^2 \rangle - \langle P \rangle^2\right)}}$$

where <…> denotes averaging with respect to the ensemble. The time t here, concerning the ENSO-IM teleconnection, is discrete with yearly increments, as explained above; this is why we write "instantaneous" using quotation marks.

Our choice corresponds to investigating the direct, i.e., non-lagged influence of ENSO on the IM. There also exists an indirect influence (Wu et al., 2012) between the beginning of a given ENSO period (from December to February) and the consecutive Indian summer monsoon. Interestingly, the sign of the correlation coefficient between the ENSO characteristic and the IM precipitation is opposite in this case. Beyond these influences, Wu et al. (2012) also identify a "coherent" influence, with origins in both seasons. These alternatives are, however, out of the scope of the present paper.

4.2 Numerical results

Since the temporal character of the forcing is quite different in certain ensembles, the results are more easily compared if we plot them as a function of the radiative forcing Q instead of time. One should keep in mind, however, that the response is always expected to exhibit some

Accepted for publication in *Journal of Climate*. DOI 10.1175/JCLI-D-19-0341.1.

delay (Herein et al., 2016), and that the nominal radiative forcing Q is just a proxy for the aggregated effects of different forcing agents (see Section 2; this can also be formulated in a rather rigorous way using the formalism of response theory, see discussion in (Lucarini et al., 2017)).

The results are shown in this representation in Fig. 2 (a,b) for all ensembles considered. Due to the moderate size of the ensembles, especially for the CESM-LE, but also strongly affecting the MPI-ESM ensembles, the numerical fluctuation of the signals is considerable, so much that one cannot read off meaningful coefficients for particular years (corresponding to individual data points in our representation). The structure of the time-dependence thus remains hidden. What might be identified, however, from our plots are main trends or their absence, with approximate values on a coarse-grained temporal resolution. Had our ensembles been of infinite size and, thus, able to accurately describe the distribution supported by the snapshot attractor, we would be able to have information at all time scales.

As shown in Fig. 2 the MPI-ESM ensembles seem to give a rather constant value, $|r|\approx 0.5$, for the coefficient (both with Niño 3 (T_{N3}) and SOI (p_{diff})), both when plotted as a function of Q (panels (a,b)) and when plotted as a function of the time t (panels (c,d)). By a visual inspection, no trends can be identified with "confidence" even for the MPI-RCP8.5E or the MPI-1pctE. The magnitude and the sign of the correlation coefficients are in harmony with the observations (Walker and Bliss, 1937; Parthasarathy and Pant, 1985; Yun and Timmermann, 2018). At the same time, the CESM shows very little correlation. Such a large discrepancy is unexpected. For this reason we do not examine the CESM here any further. Note that the underestimation of the strength of the teleconnection by the CESM agrees with Ramu et al. (2018).

Accepted for publication in *Journal of Climate*. DOI 10.1175/JCLI-D-19-0341.1.

After the visual inspection, we take to formally testing if we can reject with high confidence the hypothesis that the correlation coefficient is constant during the timespan of the MPI-ESM simulations, or in any (sub)intervals. Our test is based on the fact that the distribution of the Fisher-transform (Fisher, 1915; 1921) of an estimate of a given correlation coefficient *r* (i.e., its area-hyperbolic tangent, which we shall denote by *z*) calculated from a sample (in our case, an ensemble) of given size *N* follows a known distribution to a very good approximation: a Gaussian with a standard deviation of $1/\sqrt{N-3}$, provided that the original quantities also follow Gaussian distributions (Fisher, 1936). Should the latter conditions be met, the sampling distribution of *z* would be the same in each year of a given ensemble simulation with the only possible difference appearing in the mean of this distribution. Since calculations described in Part III of the Supplementary Material support that different years are independent for this exceptional, single variable, the setup would become suited for a Mann-Kendall test (Mann, 1945; Kendall, 1975) for the presence of a monotonic trend in the time series of *z*, whereby stationarity would become rejectable. (Note that non-monotonic time dependence is out of the scope of a single Mann-Kendall test, but testing in different intervals may reveal non-monotonicity, as discussed below.) To keep simplicity, we evaluate Mann-Kendall tests for *z* calculated from the original variables in the main text, and give support for the negligible effect of their non-Gaussianity in Part IV of the Supplementary Material.

We present values of the test statistic (Z_{MK}) to indicate the certainty of the presence of trends and also the sign of detected trends (and show the more commonly used p-values in Part V of the Supplementary Material). We carry out the test in all possible subintervals of our time series (of annual data points) in order to gain some insight into the possible inner structure of the simulations. Note that this representation suffers from the so-called multiple hypothesis

Accepted for publication in *Journal of Climate*. DOI 10.1175/JCLI-D-19-0341.1.

testing problem enhanced by correlation between neighboring data points of the plot (Wilks, 2016), i.e., even larger seemingly significant patches may be false detections. However, the point-by-point values of the test statistic are not corrupted, so that the probabilities associated to these values are correct and can be interpreted in the usual way. Results for Z_{MK} in the MPI-HE and the MPI-RCP8.5E stitched together can be seen in panels (a) and (b) of Fig. 3. Such a diagram could indicate if a trend is *linear* in time, because in that case a stratification of the color chart would be parallel to the diagonal or the hypotenause of the right triangle of color. In contrast with this, a "hockey-stick"-like time dependence would instead result in a horizontal contour of low p-values, in association with the start year of the steep change. A further relevant pattern will be a "dipole" of Z_{MK} with an axis parallel to the diagonal, corresponding to the emergence and the subsequent reversal of a trend (a "bump" or a "ditch"). Note that these features are *temporal*, as opposed to a possible relationship with the forcing (which might be represented e.g. by the radiative forcing Q, which is not a linear function of time according to Fig. 1).

A steady increase in the teleconnection strength is an attribute more so when Niño 3 characterizes ENSO (as in panel (a)) as opposed to the SOI (panel (b)). In fact, with the SOI a change is not even detected under the RCP8.5 scenario alone, only if the historical period is included. A very certain trend begins within the historical period, in the late 20th century, and can be detected almost irrespectively of the starting point of the interval, like a "hockey stick". This is unexpected, as the historical forcing is the weaker one. It is even more interesting to notice a trend with an opposite sign a few decades later: as indicated by the "dipole" structure, the teleconnection first becomes stronger, then loses strength. Note the contrast with the Niño 3-based characterization for which hard significant trends are traced

Accepted for publication in *Journal of Climate*. DOI 10.1175/JCLI-D-19-0341.1.

out only in the late 21st century: trends in the late 21st century are practically absent when using the SOI.

To support the reliability of our methodology, we present analogous results obtained with an independent hypothesis testing technique in Part V of the Supplementary Material. In a completely different approach, the slopes of linear fits displayed in similar diagrams also trace out the same structure as that of panels (a) and (b) of Figs. 3, see panels (c) and (d) of the same figure. Even a small-scale organization of the diagrams along vertical and horizontal lines proves to be the same, which suggests that this organization is not an artifact of the methodologies, but is presumably due to the influence of the more outlying values of *z*.

The diagrams of the slopes in Figs. 3(c) and (d) also give us a first estimate for the strength of assumed monotonic trends. Of course, these are very unreliable along the main diagonal (cf. the high absolute values of Z_{MK} in Figs. 3(a) and (b)), but, in statistically significant areas of the plots, show how sudden the increase and the drop in the teleconnection strength is for the SOI, and that the strengthening is particularly fast in the late 21st century for Niño 3.

As a test of robustness, we carry out the same evaluation but exclude September from the monsoon season. The diagrams of the test statistic Z_{MK} (informing about the certainty of the presence of a trend by being normally distributed in the absence of a monotonic trend) and the slopes of linear fits are displayed in Fig. 4. We conclude that the general structure of the changes in the correlation coefficient is robust, even if the detectability of change in some specific intervals is not robust.

Accepted for publication in *Journal of Climate*. DOI 10.1175/JCLI-D-19-0341.1.

In order to link what is seen when using Niño 3 and the SOI, we extend our analysis to two further ENSO characteristics: the Niño 3.4 index, considering the SST further west in the Equatorial Pacific (in the box [5°N-5°S, 170°W-120°W]; Ashok et al., 2007), and the box-SOI, extending the box concept to the atmospheric sea level pressure difference (replacing Tahiti and Darwin by the boxes [5°N-5°S, 80°E-160°E] and [5°N-5°S, 160°W-80°W], respectively; Power and Kociuba, 2010). The results for these two choices, shown in Fig. 5, are surprisingly similar to each other, and, furthermore, exhibit the main features of both of the original choices: a gradual increase in the teleconnection strength with an enhancement in the late 21st century (Niño 3) and a "bump" at the turn of the century (SOI). It is thus obvious that both Niño 3.4 and the box-SOI are some kind of intermediate representation of the ENSO phase between Niño 3 and the SOI from the point of view of the teleconnection with the Indian monsoon.

We further extend our analysis by performing the same evaluation for the MPI-1pctE and for the combination of the MPI-HE and the MPI-RCP2.6E, see Figs. 6 and 7, respectively. When using Niño 3, a long-term increase in the teleconnection strength is seen under any forcing. It is remarkable that the strength of the teleconnection keeps increasing even after the peak in the radiative forcing of the RCP2.6 (Fig. 7). When following the RCP2.6 after the historical period, the SOI-based characterization, surprisingly, also "sees" this increasing teleconnection strength in the late 21st century very well, unlike for the RCP8.5 (Fig. 3). Finally, the MPI-1pctE is completely different from the SOI point of view: the "dipole" pattern indicates a weakening followed by a strengthening.

Accepted for publication in *Journal of Climate*. DOI 10.1175/JCLI-D-19-0341.1.

5. The ENSO-IM teleconnection in view of observational data

In the context of observations, one is provided with a single historical realization, and therefore no ensemble-wise statistics can be evaluated. The obvious way to check a change in time is to compare statistics belonging to nonoverlapping time windows. A time series can even be obtained by a moving window statistics. There are two approaches to calculating moving cross-correlations. One is a direct approach, calculating Pearson's correlation coefficient in any given time window. This way the segment of the time series is "normalized" naturally by the average and standard deviation of this segment. Because of the removal of the mean, this is sometimes viewed as detrending, beside a filtering out of low-frequency variability. Yun & Timmermann (2018) (YT18 in the following) present their result in their Fig. 1 (b) following this approach. Alternatively, Krishna Kumar et al. (1999) (KK99 in the following) preprocesses the time series, before applying the direct method, by subtracting a smoothed running mean in a centred window. We note that with the latter approach, the resulting moving correlation time series is shorter by a window size.

We apply both of these algorithms here, employing a 21-year window, as did KK99 and YT18. Although, we use a centred window for evaluating the correlation itself, unlike YT18 (and probably also KK99) did without justification. Stages and the result of this are shown in Fig. 8, where we used the ERSST v5 (Huang et al., 2017) and the AISMR (Parthasarathy et al., 1994; Mooley et al., 2016) observational data products for the SST and Indian summer monsoon rainfall, respectively.

Our results do more or less reproduce that of KK99, except perhaps that we see more variability before 1980. (On the weakening of the teleconnection in the late 20th century see

Accepted for publication in *Journal of Climate*. DOI 10.1175/JCLI-D-19-0341.1.

443 also (Kinter et al., 2002; Sarkar et al. 2004; Boschat et al., 2012).) It turns out also that the
444 direct method (YT18) results in approximately the same time series in this scenario, except
445 that r is most typically, but not always, larger.
446
447 Nevertheless, we examine the robustness of the "significance" of the weakening of the
448 running correlation. Prompted by the diversity of variables used in the literature, we "perturb"
449 both the precipitation and SST variable to be correlated with one another, whose results are
450 shown in panel (a) and (b) of Fig. 9, respectively. By "perturbation" we mean considering
451 alternatives either to the data product or the area over which we calculate the mean.
452
453 To start with, instead of the AISMR data, we use the CRU PRE v4.03 (Harris, 2019) data
454 (available only over land), masked with the AISMR regions for an exact match in this respect.
455 The different data product does make a difference with respect to the "significance" of
456 weakening, indicating less of it in view of the CRU PRE data. It also matters if instead of a
457 mask given by the shape of India (except for a few states; see Fig. 1 of (Parthasarathy et al.
458 1994)) we take the mean in the box [5°N–25°N, 70°E–90°E] (Yun & Timmermann, 2018):
459 there is less (more) weakening after 1980 (around 1950). Furthermore, excluding the
460 monsoon rain in September also results in more weakening around 1950. Otherwise, the little
461 difference after 1980 prompts that in this period the monsoon season became shorter.
462
463 Using other data products for the SST, on the other hand, namely, ERSST v4 (Huang et al.
464 2015) (as also used by (Yun & Timmermann, 2018)) and HadISST1 (Rayner et al., 2013),
465 makes a difference only before 1940. Finally, considering only the eastern half of the Niño 3
466 box sees again less weakening after 1980, but leaves the period around 1950 largely
467 unaffected. (We have checked that the subtraction of a smoothed running mean before

Accepted for publication in *Journal of Climate*. DOI 10.1175/JCLI-D-19-0341.1.

calculating the running correlation (KK99) brings about minuscule difference in all cases; results not shown.)

6. Discussion

6.1 Possible reasons for the apparent discrepancy between model and observations

The contrast between the ensemble-wise (Sec. 4) and temporal (Sec. 5) results obtained for the MPI-ESM and observations, respectively, is constituted by the opposite sign of the change in the strength of the ENSO-IM teleconnection. This disagreement may have different reasons:

1. The ensemble-wise and temporal correlation coefficients do not quantify the same thing.
2. The temporal single-realisation result features so much internal variability that it does not actually allow for detecting nonstationarity.
3. The model is not truthful to the real climate.

Regarding point 1 we recall that the ensemble-wise correlation coefficient is an "instantaneous" (yearly) quantity while the temporal correlation coefficient is obviously using information from several years. The latter is not really relevant in a changing climate, whereas the probability of the co-occurrence of the anomalies of the two system components (ENSO and IM) is reflected correctly only in the former, as discussed in the Introduction.

As a further aspect of the difference, the ensemble-wise *r*, unlike the temporal one, does not exclude correlations of low-frequency variability; in principle it could be the case that the

Accepted for publication in *Journal of Climate*. DOI 10.1175/JCLI-D-19-0341.1.

493 latter was strengthening in the 20th c. and it dominated over a weakening correlation of
494 higher-frequency variability.
495
496 Regarding point 2 we remark that in Sec. 5 we did not pursue hypothesis testing (like we did
497 in Sec. 4) as the time series of moving correlations has an autocorrelation time determined by
498 the window size, and so it does not satisfy e.g. the assumption of the MK test. While this may
499 be circumvented by restricting the investigation to non-overlapping windows, such a
500 technique makes obvious that the autocorrelation introduced by windowing seriously reduces
501 the effective sample size. For instance, even if the original time series of r lacks
502 autocorrelation, a 21-year windowing of a 140-year time series results in an effective sample
503 size of no more than 7, approximately. Nevertheless, it is surprisingly common to see in
504 publications an incorrect report on the significance of e.g. trends despite these aspects. It
505 appears to us that KK99 also disregarded these considerations when claimed that the
506 weakening of the teleconnection is significant in a statistical sense. Indeed, if the detection of
507 trends or nonstationarity in this context is already challenging when endowed with a 63-
508 member ensemble (Sec. 4), it seems hopeless from a single realization. See also Wunsch
509 (1999), Gershunov et al. (2001), Yun and Timmermann (2018).
510
511 Nevertheless, it would be very valuable to be able to rely on temporal statistics, by which
512 observational climate data could be analyzed. As climate models can represent some aspects
513 of the climate inaccurately, our only chance to gain an understanding of those aspects is by
514 analyzing observational data. Ben Santer advocates (conference contribution) that the great
515 value of ensembles of climate model simulations, like the MPI-GE or CESM-LE, is that they
516 can serve as a test-bed for temporal statistics or algorithms. For example, one can check how

Accepted for publication in *Journal of Climate*. DOI 10.1175/JCLI-D-19-0341.1.

well ergodicity is satisfied in some given context, which is known (Drótos et al. 2016) to be not satisfied in a generic nonautonomous case.

Returning to point 1 in this respect, we can simply evaluate the temporal correlations for all 63 converged members of the MPI-GE, and see if they typically feature a *weakening* teleconnection like KK99 reported. Fig. 10 shows the result with both kinds of "detrending". We see that the ensemble average temporal correlation (a quantity also evaluated by Mamalakis et al. (2019)) is rather steadily *increasing* in the historical period, which lets us conclude that the disparate treatment of low-frequency correlations does not bring about a typical opposite trend here. Nevertheless, the different behavior of the ensemble-mean temporal correlation under RCP8.5 – increasing with the indirect method of KK99 and stagnating with the direct method of YT18 – cautions us to keep an open mind about unexpected differences.

The same figure also addresses the possibility of point 2. The variances of the moving correlations are very large, but it is also not very unlikely to have a smaller variance for many decades followed by a drift, i.e., a considerable apparent weakening or strengthening of the teleconnection. We find examples for this among the 63 ensemble members. Actually, it is recognized in many studies (Kinter et al., 2002; Ashrit et al., 2003; Sarkar et al. 2004; Ashrit et al., 2005; Annamalai et al., 2007; Kitoh, 2007; Chowdary et al., 2012; Li and Ting, 2015) that "modulations" and corresponding apparent trends in the studied correlation coefficient, when calculated over different time intervals (as done by e.g. Boschat et al. (2012) and Ruiqing et al. (2015)) or over moving (sliding) time windows (as done by e.g. Krishna Kumar et al. (1999), Ashrit et al. (2001), Kinter et al. (2002), Ashrit et al. (2003), Ashrit et al. (2005), Annamalai et al. (2007), Kitoh (2007), Chowdary et al. (2012), Li and Ting (2015)), can

Accepted for publication in *Journal of Climate*. DOI 10.1175/JCLI-D-19-0341.1.

appear as a result of internal variability. In particular, Li and Ting (2015) conclude that the observed weakening of the teleconnection in the late 20th century would be due to internal variability. Sarkar et al. (2004) go beyond this saying, on the basis of physical arguments, that "the effect of ENSO on Indian precipitation has not decreased but on the contrary it has increased in recent times", aligning, in fact, to our finding in the MPI-GE, but claiming that actual strenghtening was dominated by internal variability seeing a weakening.

Finally, we address the possibility of model errors, point 3. We start with presenting maps of global SST trends for the historical period, in Fig. 11, comparing the MPI-ESM and observations. All-year data is used to fit a straight line whose slope represents the trend. As for the model, we show both the ensemble average and standard deviation of the trends.

Like some earlier version (Collins, 2004), the version of the MPI-ESM used to generate the MPI-GE seems to have a La-Niña-like warming, that is, more warming in the Western Equatorial Pacific versus the Eastern'. Considering the ensemble-wise variance globally, the observed warming (and cooling) trends seem to be consistent with the model. Note that the observed Equatorial Pacific warming, like the ensemble mean in the MPI-GE, is La-Niña-like, and it is in disagreement with the report of Lian et al. (2018) on a cooling instead, even if in the Eastern Equatorial Pacific. We do not pursue here rigorously (Wilks, 2016) the question of (in)consistency of these patterns; although it should be clear that it would be just a matter of data set size to detect inconsistency.

We continue with similar maps of JJAS precipitation climatology over India shown in Fig. 12. It is clear that the model has less rain, possibly partly because of its coarser resolution, so that high mountains that "force" precipitation are not resolved. Increasing model resolution has

Accepted for publication in *Journal of Climate*. DOI 10.1175/JCLI-D-19-0341.1.

been plausibly indicated by Anand et al. (2018) to reduce model biases (see their Fig. 6), also over the sea. The latter might be a clue that, due to the conservation of water, negative precipitation bias over high mountains and positive biases nearby over the ocean can be related. Considering the ensemble-wise variability too, the discrepancy can be indeed considered a bias, not just a difference by chance or statistical error. However, the patterns between model and observations certainly bear a resemblance. The patterns for the trends, on the other hand, are less similar; see Fig. 13. Furthermore, the magnitude of some local trends in the observation exceeds by far anything in any realization of the model.

While this might be a clue to the origin of the discrepancy between a possible weakening temporal correlation in observations and a typically strengthening one in the model, we emphasize that a temporal correlation of detrended data is hoped to quantify some relationship between fluctuations rather than forced trends of the climatic mean signal. Nevertheless, in conclusion, if the discrepancy is to do with model errors (point 3), then it is more likely coming from the side of precipitation than SST.

However, when regarding the particular quantities at the basis of our analyses of the teleconnection, Fig. 14 (a) shows that the average Indian monsoon rainfall in the model and observations seem to have consistent fluctuation characteristics and perhaps also trend, even though the underestimation of the rainfall by the model is also seen from this angle. The Niño 3 index or T_{N3}, shown in panel (b), can be described very similarly: despite a 2 $^{\circ}$C warmer model, the variance and temporal characteristics of the fluctuations seem to closely resemble each other in the model and observations.

Accepted for publication in *Journal of Climate*. DOI 10.1175/JCLI-D-19-0341.1.

6.2 The nonlinearity of the response and possible reasons for that

In view of the Niño 3-AISMR correlation (see e.g. the (a) panels of Fig. 3, 4, 6) the possibility that the forced response of the teleconnection would be approximately linear cannot be excluded. However, representing ENSO by the sea surface temperature just in a somewhat more westerly box (Niño 3.4), nonlinearity, what is more, non-monotonicity becomes obvious (see the (b) panels of the same figures). We shall first discuss possible reasons for nonlinearity even if the forcing might be considered relatively weak in all scenarios (from the point of view of response theory (Ruelle, 2009; Lucarini et al., 2017)). Remember that temporal linearity has to be distinguished from a linear response to forcing, but non-monotonicity in Fig. 5 excludes both options. We also recall that the teleconnection keeps strengthening even after radiative forcing peaks in the RCP2.6 (see Fig. 7).

In the slightly different setup of (Herein et al., 2018), considering precipitation only in the *northern* part of India, from an analysis of the sensitivity of hypothesis tests to stationarity, we concluded that the strength of the teleconnection in view of the SOI cannot respond to the radiative forcing Q instantaneously and linearly, since otherwise those tests would have had to detect nonstationarity also in the MPI-RCP8.5E alone and the MPI-1pctE (beyond the MPI-HE), which was not the case. Some very strong form of nonlinearity could explain the results in principle. However, another possible explanation lies in the radiative forcing Q not being a dynamical forcing, i.e., a single quantity that appears explicitly in the equations of motion. That is, a causal response function might not exist between Q (as predictor) and r (as predictand; Lucarini, 2018).

Accepted for publication in *Journal of Climate*. DOI 10.1175/JCLI-D-19-0341.1.

In particular, the strength of the teleconnection may respond in a different way to variations in different forcing agents. Remember that the nominal radiative forcing Q represents the aggregated effects from several different agents, and responses might not be possible to be interpreted in terms of variations in the single quantity Q. The underlying mechanisms might even turn out to be not or not directly related to the increase in the net energy flux.

In fact, the differentiation of responses with respect to different forcing agents would not be very surprising. As shown by Bódai et al. (2018) by considering a (globally homogeneous) CO_2 forcing alone, while the resulting Q might act as a dynamical forcing with respect to the surface temperature, it does not do so e.g. with respect to the temperature at the tropopause (Bódai et al., 2018). The teleconnection of ENSO with the Indian summer monsoon might indeed involve a physical mechanism not restricted to the surface, or to observables that would secure the causality of the "response" of the teleconnection to Q. If we add that the response in the climatic mean of the Indian summer monsoon has actually been found by Li et al. (2015; utilizing techniques based on temporal averaging, though) to be governed by different mechanisms under aerosol forcing (related to volcanism, or, indeed, large scale pollution in South and South-East Asia) and greenhouse-gas forcing, we can easily imagine that the fluctuations of the Indian summer monsoon respond differently to these two kinds of forcings, causing the teleconnection to respond in a different way, too.

Note that volcanism is enhanced in the late 20^{th} century when changes in the strength of the teleconnection are first prominently seen in the MPI-GE. In fact, a hypothesis has been put forward by Maraun and Kurths (2005) that after major volcano eruptions in the Southwest Pacific the "cooling effect could reduce the land/sea temperature gradient and thus make the Monsoon more sensitive to ENSO influence". These authors found more regular oscillatory

Accepted for publication in *Journal of Climate*. DOI 10.1175/JCLI-D-19-0341.1.

ENSO dynamics and a phase locking between ENSO and the monsoon in the observed time series after major volcano eruptions in southern Indonesia, which, they claim, should be reflected in an increased correlation, perhaps (see below) consistent with our finding. This could also be an indication that a single realization contains already a lot of information about the forced response in terms of a nonlinear quantifier of the teleconnection, as opposed to Pearson's "linear" correlation coefficient. Taking into account that the pure ensemble-based description of teleconnections is the statistically most relevant one and is usually more robust than single-realization temporal techniques, it might prove to be extremely fruitful to carry out an ensemble-based analysis but replacing Pearson's correlation coefficient by e.g. Spearman's "nonlinear" rank correlation coefficient.

Nevertheless, Maraun and Kurths (2005) claim to not disagree with KK99 about the decrease of the correlation strength as a forced response. They describe a transition near 1980 from a 1:1 phase locking into a 2:1 phase locking, with the Indian monsoon oscillating twice as fast. This connection, they claim, would be "invisible to (linear) correlation analysis", or rather the correlation would be destructed by the additional monsoon peak. Note, however, that nonstationarity is not yet verified for observations (Sec. 6.1), so that the picture might be more complicated than sketched by Maraun and Kurths (2005). From this point of view, it could be checked if the MPI-ESM features the same effect in terms of the phase difference analysed by them.

The above discussion shows many possibilities for a nonlinear response. However, we have also found considerable variations in the results when choosing different characteristics of ENSO. Nevertheless, a long-term increase in the ENSO-IM teleconnection strength is present in *every* scenario when utilizing an area-based index. Furthermore, a "bump" is also rather

Accepted for publication in *Journal of Climate*. DOI 10.1175/JCLI-D-19-0341.1.

consistently detected under the combination of the historical and RCP8.5 forcings at the turn of the century if the ENSO characteristic is based on some more western part of the Pacific. It is only for the pressure difference p_{diff} between two gridpoints that a rather erratic behavior is found. Such a quantity should be more sensitive when the spatial patterns playing the main role in the teleconnection phenomenon are not simple and when these patterns change substantially even if the bulk does not.

While the analysis of changes in the ENSO pattern (usually investigated by emprical orthogonal functions (EOFs)) may already prove to be informative, the patterns most relevant for the teleconnection can be identified by the "maximal covariance analysis" (MCA) or "canonical correlation analysis" (CCA). One can evaluate these also ensemble-wise, similarly to the recently developed snapshot EOF technique (SEOF (Haszpra et al., n.a.); see its application to ENSO in (Herein et al., 2019); one may call the new techniques SMCA and SCCA), by which changes in these patterns can be studied or detected. In principle, it may still be that such analyses yield a different picture depending on using the SST or the sea-level pressure to characterize ENSO. We will investigate these matters as future work.

Acknowledgement

The authors wish to express gratitude to J. Broecker, C. Franzke, T. Haszpra, T. Kuna, N. Maher, S. Milinski, and T. Tél for useful remarks and discussions. GD is thankful to B. Stevens, T. Mauritsen, Y. Takano, and N. Maher for providing access to the output of the MPI-ESM ensembles. The authors also wish to thank the Climate Data Gateway at NCAR for providing access to the output of the CESM-LE. The constructive feedback from three reviewers is greatly acknowledged, most importantly their suggestion of considering an SST-

Accepted for publication in *Journal of Climate*. DOI 10.1175/JCLI-D-19-0341.1.

based index, beside the sea-level-pressure-based SOI, to represent ENSO. TB wishes to thank Kyung-Sook Yun for sharing with him some of the preprocessed observational data used in (Yun & Timmermann, 2018) and pointing him to other data sources.

Funding

The simulations for the MPI-RCP8.5E were supported by the H2020 grant for the CRESCENDO project (grant no. 641816). MH is thankful for the great support of the DFG Cluster of Excellence CliSAP. This research was supported by the National Research, Development and Innovation Office — NKFIH under grants PD124272, K125171 and FK124256. GD was supported by the Ministerio de Economía, Industria y Competitividad of the Spanish Government under grant LAOP CTM2015-66407-P (AEI/FEDER, EU). TB, VL and FL were supported by the H2020 grants for the CRESCENDO (grant no. 641816) and Blue-Action (grant no. 727852) projects. VL has been supported by the DFG Sfb/Transregio TRR181 project. TB was also supported by the Institute for Basic Science (IBS), under IBS-R028-D1.

Accepted for publication in *Journal of Climate*. DOI 10.1175/JCLI-D-19-0341.1.

References

Anand, A., Mishra, S.K., Sahany, S. et al. Indian Summer Monsoon Simulations: Usefulness of Increasing Horizontal Resolution, Manual Tuning, and Semi-Automatic Tuning in Reducing Present-Day Model Biases. Sci Rep 8, 3522 (2018) doi:10.1038/s41598-018-21865-1

Annamalai, H., K. Hamilton, and K.R. Sperber, 2007: The South Asian Summer Monsoon and Its Relationship with ENSO in the IPCC AR4 Simulations. *J. Climate*, 20, 1071–1092, https://doi.org/10.1175/JCLI4035.1

Arnold, L. Random Dynamical Systems (Springer-Verlag, Berlin, Germany, 1998).

Ashok, K., Behera, S. K., Rao, S. A., Weng, H., and Yamagata, T. (2007), El Niño Modoki and its possible teleconnection, *J. Geophys. Res.*, 112, C11007, doi:10.1029/2006JC003798.

Ashrit, R.G., Rupa Kumar, K., Krishna Kumar, K. (2001). ENSO-Monsoon relationships in a greenhouse warming scenario. Geophys. Res. Lett. 28. 9, 1727-1730.

Ashrit, R.G., H. Douville, K. Rupa Kumar (2003). Response of the Indian Monsoon and ENSO-Monsoon Teleconnection to Enhanced Greenhouse Effect in the CNRM Coupled Model. Journal of the Meteorological Society of Japan. 81. 4, 779-803.

Ashrit, R.G., A. Kitoh, S. Yukimoto, Transient Response of ENSO-Monsoon Teleconnection in MRI-CGCM2.2 Climate Change Simulations, Journal of the Meteorological Society of

Accepted for publication in *Journal of Climate*. DOI 10.1175/JCLI-D-19-0341.1.

Japan. Ser. II, Released July 27, 2005, Online ISSN 2186-9057, Print ISSN 0026-1165, https://doi.org/10.2151/jmsj.83.273

Bellenger H, Guilyardi E, Leloup J, Lengaigne M, Vialard J (2014). ENSO representation in climate models: from CMIP3 to CMIP5. Clim. Dyn. 42:1999–2018.

Bjerknes, J. Atmospheric teleconnections from the equatorial Pacific. (1969) Mon. Weather Rev. 97, 163–172.

Bittner, M., Schmidt, H., Timmreck, C., and Sienz, F. (2016). Using a large ensemble of simulations to assess the Northern Hemisphere stratospheric dynamical response to tropical volcanic eruptions and its uncertainty. Geophys. Res. Lett. 43, 9324–9332.

Bódai, T., Károlyi, G. & Tél, T. Fractal snapshot components in chaos induced by strong noise. (2011) Phys. Rev. E 83, 046201.

Bódai, T. and Tél, T.. Annual variability in a conceptual climate model: Snapshot attractors, hysteresis in extreme events, and climate sensitivity. (2012) Chaos, 22:023110.

Bódai, T., Lucarini, V., and Lunkeit, F.: Critical Assessment of Geoengineering Strategies using Response Theory, Earth Syst. Dynam. Discuss., https://doi.org/10.5194/esd-2018-30, in review, 2018.

Boschat G., Terray P., Masson S. (2012). Robustness of SST teleconnections and precursory patterns associated with the Indian summer monsoon. Clim. Dyn. 38. 11, 2143-2165.

Accepted for publication in *Journal of Climate*. DOI 10.1175/JCLI-D-19-0341.1.

Branstator, G. and H. Teng (2010) Two Limits of Initial-Value Decadal Predictability in a CGCM. *J. Climate*, **23**, 6292–6311, https://doi.org/10.1175/2010JCLI3678.1

Cai W.-J., A. Santoso, G.-J. Wang, S. Yeh, S. An, K. Cobb, M. Collins, E. Guilyardi, F. Jin, J. Kug, M. Lengaigne, M. J. McPhaden, K Takahashi, A. Timmermann, G. Vecchi, M. Watanabe, and L.-X. Wu, 2015: ENSO and Greenhouse Warming. Nature Climate Change, doi: 10.1038/NCLIMATE2743.

Capotondi A. (2013) ENSO diversity in the NCAR CCSM4 climate model. J. Geophys Res 118:4755–4770.

Chekroun, M. D., Simonnet, E. and Ghil, M. (2011). Stochastic climate dynamics: Random attractors and time-dependent invariant measures. Physica D, 240:1685–1700.

Chowdary, J.S., Xie S., H. Tokinaga, Y.M. Okumura, H. Kubota, N. Johnson, and X. Zheng, (2012). Interdecadal Variations in ENSO Teleconnection to the Indo–Western Pacific for 1870–2007. J. Climate, 25, 1722–1744

Christensen, J.H., K. Krishna Kumar, E. Aldrian, S.-I. An, I.F.A. Cavalcanti, M. de Castro, W. Dong, P. Goswami, A. Hall, J.K. Kanyanga, A. Kitoh, J. Kossin, N.-C. Lau, J. Renwick, D.B. Stephenson, S.-P. Xie and T. Zhou (2013): Climate Phenomena and their Relevance for Future Regional Climate Change. In: Climate Change 2013: The Physical Science Basis. Contribution of Working Group I to the Fifth Assessment Report of the Intergovernmental Panel on Climate Change [Stocker, T.F., D. Qin, G.-K. Plattner, M. Tignor, S.K. Allen, J.

Accepted for publication in *Journal of Climate*. DOI 10.1175/JCLI-D-19-0341.1.

Boschung, A. Nauels, Y. Xia, V. Bex and P.M. Midgley (eds.)]. Cambridge University Press, Cambridge, United Kingdom and New York, NY, USA.

Collins, M. & The CMIP Modelling Groups (BMRC (Australia), CCC (Canada), CCSR/NIES (Japan), CERFACS (France), CSIRO (Austraila), MPI (Germany), GFDL (USA), GISS (USA), IAP (China), INM (Russia), LMD (France), MRI (Japan), NCAR (USA), NRL (USA), Hadley Centre (UK) and YNU (South Korea)) Clim Dyn (2005) 24: 89. https://doi.org/10.1007/s00382-004-0478-x

Collins, M., An, S.-I., Cai, W., Ganachaud, A., Guilyardi, E., Jin, F.-F., Jochum, M., Lengaigne, M., Power, S., Timmermann, A., Vecchi, G., Wittenberg, A. (2010) The impact of global warming on the tropical Pacific Ocean and El Niño. Nature Geoscience 3, 391 – 397.

Daron, J. D. and Stainforth, D. A. (2015). On quantifying the climate of the nonautonomous Lorenz-63 model. Chaos, 25:043103.

Deser, C., Phillips, A., Bourdette, V. and Teng, H. (2012). Uncertainty in climate change projections: the role of internal variability, Clim. Dyn. 38, 527—546.

Dijkstra H. A. 2005 Nonlinear Physical Oceanography, Springer.

Drótos, G., Bódai, T., Tél, T. (2017) "On the importance of the convergence to climate attractors". Eur. Phys. J. Spec. Top. 226, 2031-2038.

Accepted for publication in *Journal of Climate*. DOI 10.1175/JCLI-D-19-0341.1.

807 Drótos, G., Bódai, T., Tél, T. (2015) Probabilistic concepts in a changing climate: A snapshot
808 attractor picture. Journal of Climate 28, 3275–3288.
809
810 Drótos, G., Bódai, T., Tél, T. (2016) Quantifying nonergodicity in nonautonomous dissipative
811 dynamical systems: An application to climate change. Phys. Rev. E 94, 022214.
812
813 Fisher, R. A. (1915). "Frequency distribution of the values of the correlation coefficient in
814 samples of an indefinitely large population". Biometrika. Biometrika Trust. 10 (4): 507–521.
815 Doi:10.2307/2331838. JSTOR 2331838.
816
817 Fisher, R. A. (1921). "On the 'probable error' of a coefficient of correlation deduced from a
818 small sample". Metron. 1: 3–32.
819
820 Fisher, R. A. (1936). "Statistical Methods for Research Workers", 6th edition. Oliver and
821 Boyd, Edinburgh and London, UK.
822
823 Freychet, N., H.-H. Hsu, C. Chou, and C.-H. Wu, (2015). Asian summer monsoon in CMIP5
824 projections: A link between the change in extreme precipitation and monsoon dynamics. J.
825 Climate, 28, 1477-1493.
826
827 Gershunov, A., N. Schneider, and T. Barnett, 2001: Low-Frequency Modulation of the
828 ENSO–Indian Monsoon Rainfall Relationship: Signal or Noise? J. Climate, 14, 2486–2492
829
830 Ghil, M. , Chekroun, M. D. and Simonnet, E., (2008). Climate dynamics and fluid
831 mechanics: Natural variability and related uncertainties. Physica D, 237:2111–2126.

Accepted for publication in *Journal of Climate*. DOI10.1175/JCLI-D-19-0341.1.

Giorgetta, M. A., et al. (2013). Climate and carbon cycle changes from 1850 to 2100 in MPI-ESM simulations for the Coupled Model Intercomparison Project phase 5. J. Adv. Model. Earth Syst., 5, 572–597.

Guilyardi, E. et al. (2009) Understanding El Niño in ocean–atmosphere General Circulation Models: progress and challenges. Bull. Am. Meteorol. Soc.90, 325–340.

Ian Harris, RELEASE NOTES FOR CRU TS v4.03: 15 May 2019, https://crudata.uea.ac.uk/cru/data/hrg/cru_ts_4.03/Release_Notes_CRU_TS4.03.txt https://crudata.uea.ac.uk/cru/data/hrg/cru_ts_4.03/cruts.1905011326.v4.03/pre/

Haszpra, T., Topál, D., and Herein, M. (n.a.) On the time evolution of the Arctic Oscillation and related wintertime phenomena under different forcing scenarios in an ensemble approach (submitted to the Journal of Climate).

Hedemann, C., Mauritsen, T., Jungclaus, J., and Marotzke, J. (2017). The subtle origins of surface-warming hiatuses. Nature Climate Change, 7, 336-340.

Herein, M., Márfy, J., Drótos, G., Tél, T. (2016). Probabilistic concepts in intermediate-complexity climate models: A snapshot attractor picture. J. Clim. 29(1) pp. 259-272.

Herein, M., Drótos, G., Haszpra, T., Márfy, J., and Tél, T. (2017). The theory of parallel climate realizations as a new framework for teleconnection analysis. Sci. Rep. 7, 44529; doi: 10.1038/srep44529.

Accepted for publication in *Journal of Climate*. DOI10.1175/JCLI-D-19-0341.1.

Mátyás Herein, Gábor Drótos, Tamás Bódai, Frank Lunkeit, and Valerio Lucarini (2018) Reconsidering the relationship of the El Niño—Southern Oscillation and the Indian monsoon using ensembles in Earth system models, arXiv:1803.08909

Boyin Huang, Viva F. Banzon, Eric Freeman, Jay Lawrimore, Wei Liu, Thomas C. Peterson, Thomas M. Smith, Peter W. Thorne, Scott D. Woodruff, and Huai-Min Zhang, 2015: Extended Reconstructed Sea Surface Temperature (ERSST), Version 4. NOAA National Centers for Environmental Information. Doi:10.7289/V5KD1VVF. https://data.nodc.noaa.gov/cgi-bin/iso?id=gov.noaa.ncdc:C00884#

Boyin Huang, Peter W. Thorne, Viva F. Banzon, Tim Boyer, Gennady Chepurin, Jay H. Lawrimore, Matthew J. Menne, Thomas M. Smith, Russell S. Vose, and Huai-Min Zhang (2017): NOAA Extended Reconstructed Sea Surface Temperature (ERSST), Version 5. NOAA National Centers for Environmental Information. Doi:10.7289/V5T72FNM. https://data.nodc.noaa.gov/cgi-bin/iso?id=gov.noaa.ncdc:C00927

Hurrell, J. W., et al. (2012). The community Earth system model: A framework for collaborative research, Bull. Am. Meteorol. Soc., 94, 1339–1360.

Kaszás, B., Feudel, U., and Tél, T. (2019) Tipping phenomena in typical dynamical systems subjected to parameter drift, *Scientific Reports* 9, 8654.

Accepted for publication in *Journal of Climate*. DOI 10.1175/JCLI-D-19-0341.1.

Kay et al. The Community Earth System Model (CESM) Large Ensemble project: A community resource for studying climate change in the presence of internal climate variability. (2015) Bull. Amer. Meteor. Soc., 96:1333–1349.

Kendall, M.G. 1975. Rank Correlation Methods, 4th edition, Charles Griffin, London.

Kim, W. M., S. Yeager, P. Chang, and G. Danabasoglu, 2017: Low-frequency North Atlantic climate variability in the Community Earth System Model Large Ensemble. J. Climate., doi: 10.1175/JCLI-D-17-0193.1.

Kinter, J.L., K. Miyakoda, and S. Yang, 2002: Recent Change in the Connection from the Asian Monsoon to ENSO. *J. Climate,* **15**, 1203–1215,

Kitoh A, Variability of Indian monsoon-ENSO relationship in a 1000-year MRI-CGCM2.2 simulation. Nat Hazards (2007) 42:261–272.

Krishna Kumar K, Rajagopalan B, Cane MA, On the Weakening Relationship Between the Indian Monsoon and ENSO. Science 284:2156-2159 (1999).

Lamarque J-F, Bond TC, Eyring V, Granier C, Heil A, Klimont Z, Lee D, Liousse C, Mieville A, Owen B, et al. (2010) Historical (1850–2000) gridded anthropogenic and biomass burning emissions of reactive
gases and aerosols: methodology and application. Atmos Chem Phys 10, 7017-7039.

Leith C. (1978) Predictability of climate, Nature 276, 352.

Accepted for publication in *Journal of Climate*. DOI 10.1175/JCLI-D-19-0341.1.

L'Heureux, M. L., Collins, D. C., Hu, Z.-Z. (2013). Linear trends in sea surface temperature of the tropical Pacific Ocean and implications for the El Niño-Southern Oscillation. Climate Dynamics, 40, 5, pp 1223–1236.

L'Heureux, M. L., and Ken Takahashi and Andrew B. Watkins and Anthony G. Barnston and Emily J. Becker and Tom E. Di Liberto and Felicity Gamble and Jon Gottschalck and Michael S. Halpert and Boyin Huang and Kobi Mosquera-Vásquez and Andrew T. Wittenberg (2017). Observing and Predicting the 2015/16 El Niño. Bull. Amer. Meteor. Soc., 98, 1363-1382.

Li, X., and M. Ting (2015), Recent and future changes in the Asian monsoon-ENSO relationship: Natural or forced? Geophys.Res. Lett.,42, 3502–3512, doi:10.1002/2015GL063557.

Li, X., M. Ting, C. Li, and N. Henderson (2015) Mechanisms of Asian Summer Monsoon Changes in Response to Anthropogenic Forcing in CMIP5 Models. J. Climate, 28, 4107–4125.

Tao Lian, Dake Chen, Jun Ying, Ping Huang, Youmin Tang, Tropical Pacific trends under global warming: El Niño-like or La Niña-like?, *National Science Review*, Volume 5, Issue 6, November 2018, Pages 810–812, https://doi.org/10.1093/nsr/nwy134

Lindsey, R., 2013. In Watching for El Niño and La Niña, NOAA Adapts to Global Warming. Climate.gov. ClimateWatch Magazine.

Accepted for publication in *Journal of Climate*. DOI10.1175/JCLI-D-19-0341.1.

930 Lucarini, V., Ragone, F., Lunkeit, F. (2017). Predicting Climate Change Using Response
931 Theory: Global Averages and Spatial Patterns. J. stat. Phys. 166, 3–4, 1036–1064.
932
933 Lucarini, V. (2018) Revising and Extending the Linear Response Theory for Statistical
934 Mechanical Systems: Evaluating Observables as Predictors and Predictands, J Stat Phys
935 173: 1698. https://doi.org/10.1007/s10955-018-2151-5
936
937 N. Maher, S. Milinski, L. Suarez-Gutierrez, M. Botzet, M. Dobrynin, L. Kornblueh, J. Kröger,
938 Y. Takano, R. Ghosh, C. Hedemann, C. Li, H. Li, E. Manzini, D. Notz, D. Putrasahan, L.
939 Boysen,
940 M. Claussen, T. Ilyina, D. Olonscheck, T. Raddatz, B. Stevens, J. Marotzke (2019) The Max
941 Planck Institute Grand Ensemble: Enabling the Exploration of Climate System Variability,
942 Journal of Advances
943 in Modeling Earth Systems 11, 7.
944 Antonios Mamalakis, Jin-Yi Yu, James T. Randerson, Amir AghaKouchak & Efi Foufoula-
945 Georgio (2019) Reply to: A critical examination of a newly proposed interhemispheric
946 teleconnection to Southwestern US winter precipitation, *Nature Communications* 10, 2918.
947 Mann, H.B. 1945. Non-parametric tests against trend, Econometrica 13:163-171.
948
949 Maraun, D., and Kurths, J. (2005), Epochs of phase coherence between El Niño/Southern
950 Oscillation and Indian monsoon, Geophys. Res. Lett., 32, L15709, doi:
951 10.1029/2005GL023225.
952
953 Meinshausen, M., Smith, S. J., Calvin, K., Daniel, J. S., Kainuma, M. L. T., Lamarque, J-F.,
954 Matsumoto, K., Montzka, S. A., Raper, S. C. B., Riahi, K., Thomson, A., Velders, G. J. M.,

Accepted for publication in *Journal of Climate*. DOI 10.1175/JCLI-D-19-0341.1.

van Vuuren, D.P. P. (2011). The RCP greenhouse gas concentrations and their extensions from 1765 to 2300. Climatic Change 109, 213.

D.A. Mooley, B. Parthasarathy, K. Rupa Kumar, N.A. Sontakke, A.A. Munot, D.R. Kothawale, IITM Indian regional/subdivisional Monthly Rainfall data set (IITM-IMR), June 14, 2016, ftp://www.tropmet.res.in/pub/data/rain/iitm-imr-readme.txt

Neelin, J. D., Battisti, D. S., Hirst, A. C., Jin, F. F., Wakata, Y., Yamagata, T., Zebiak, S. E. (1998) ENSO theory. J. Geophys. Res. Ocean. 103, 14261–14290.

Parthasarathy, B., Pant, G., B. (1985). Seasonal relationships between Indian summer monsoon rainfall and the Southern Oscillation. Journal of Climatology. 5, 369-378.

B. Parthasarathy, A. A. Munot, and D. R. Kothawale, All-India Monthly and Seasonal Rainfall Series: 1871-1993, Theor. Appl. Climatol. 49, 217-224 (1994)

Power, S.,B., Kociuba, G. (2011). The impact of global warming on the Southern Oscillation Index. Clim Dyn.37:1745–1754

Rayner N. A., D. E. Parker, E. B. Horton, C. K. Folland, L. V. Alexander, D. P. Rowell, E. C. Kent, A. Kaplan, Global analyses of sea surface temperature, sea ice, and night marine air temperature since the late nineteenth century, J. Geophys. Res., 108 (D14), 4407, doi:10.1029/2002JD002670, 2003.

https://www.esrl.noaa.gov/psd/gcos_wgsp/Timeseries/Data/Niño 3.long.data

Accepted for publication in *Journal of Climate*. DOI 10.1175/JCLI-D-19-0341.1.

Ramaswamy, V., O. Boucher, J. Haigh, D. Hauglustaine, J. Haywood, G. Myhre, T. Nakajima, G.Y. Shi, S. Solomon (2001): Radiative Forcing of Climate Change. In: Climate Change 2001: The Scientific Basis. Contribution of Working Group I to the Third Assessment Report of the Intergovernmental Panel on Climate Change [Houghton, J.T., Y. Ding, D.J. Griggs, M. Noguer, P.J. van der Linden, X. Dai, K. Maskell, and C.A. Johnson (eds.)]. Cambridge University Press, Cambridge, United Kingdom and New York, NY, USA, 881pp.

Ramu, D.A., Chowdary, J.S., Ramakrishna, S.S.V.S., O. S. R. U. B. Kumar. (2018) Diversity in the representation of large-scale circulation associated with ENSO-Indian summer monsoon teleconnections in CMIP5 models. Theor Appl Climatol. 132. 1-2, pp 465–478.

Rogers and Nicewander (1988). "Thirteen Ways to Look at the Correlation Coefficient". The American Statistician. 42 (1): 59–66.

Romeiras, F. J., Grebogi, C., Ott, E. (1990). Multifractal properties of snapshot attractors of random maps. Phys.Rev. A, 41:784.

Roy, I, Tedeschi, RG, Collins, M. ENSO teleconnections to the Indian summer monsoon under changing climate. *Int J Climatol*. 2019; 39: 3031–3042. https://doi.org/10.1002/joc.5999

Ruelle, D. A review of linear response theory for general differentiable dynamical systems. Nonlinearity, 22(4):855, 2009.

Accepted for publication in *Journal of Climate*. DOI10.1175/JCLI-D-19-0341.1.

Ruiqing L, Shihua L, Bo H and Yanhong G, Connections between the South Asian summer monsoon and the tropical sea surface temperature in CMIP5. Journal of Meteorological Research 29(1):106-118 (2015)

Sarkar, S., R. P. Singh, and M. Kafatos (2004), Further evidences for the weakening relationship of Indian rainfall and ENSO over India, Geophys. Res. Lett., 31, L13209, doi: 10.1029/2004GL020259.

Stevens, B. (2015), Rethinking the Lower Bound on Aerosol Radiative Forcing, J Climate, 28(12), 4794–4819, doi:10.1175/JCLI-D-14-00656.1

Suárez-Gutiérrez, L., C. Li, P. W. Thorne, and J. Marotzke (2017), Internal variability in simulated and observed tropical tropospheric temperature trends, Geophys. Res. Lett., 44, 5709–5719.

Timmermann, A., Soon-Il An, Jong-Seong Kug, Fei-Fei Jin, Wenju Cai, Antonietta Capotondi, Kim Cobb, Matthieu Lengaigne, Michael J. McPhaden, Malte F. Stuecker, Karl Stein, Andrew T. Wittenberg, Kyung-Sook Yun, Tobias Bayr, Han-Ching Chen, Yoshimitsu Chikamoto, Boris Dewitte, Dietmar Dommenget, Pamela Grothe, Eric Guilyardi, Yoo-Geun Ham, Michiya Hayashi, Sarah Ineson, Daehyun Kang, Sunyong Kim, WonMoo Kim, June-Yi Lee, Tim Li, Jing-Jia Luo, Shayne McGregor, Yann Planton, Scott Power, Harun Rashid, Hong-Li Ren, Agus Santoso, Ken Takahashi, Alexander Todd, Guomin Wang, Guojian Wang, Ruihuang Xie, Woo-Hyun Yang, Sang-Wook Yeh, Jinho Yoon, Elke Zeller, and Xuebin Zhang (2018). El Niño–Southern Oscillation complexity. Nature 559, 535–545.

Accepted for publication in *Journal of Climate*. DOI 10.1175/JCLI-D-19-0341.1.

1029 Trenberth (1984). Signal versus Noise in the Southern Oscillation. Monthly Weather Review.
1030 112,326-332.
1031
1032 Trenberth, K. E., (1976). Spatial and temporal variations of the South-ern Oscillation. Quart.
1033 J. Roy. Meteor. Soc.,102, 639–653.
1034
1035 Trenberth, K.E., 1997: The Definition of El Niño. *Bull. Amer. Meteor. Soc.*, **78**, 2771–
1036 2778, https://doi.org/10.1175/1520-0477(1997)078<2771:TDOENO>2.0.CO;2
1037
1038 Troup, A. J., (1965). The ‘‘southern oscillation.” Quart. J. Roy. Meteor.Soc., 91, 490–506.
1039
1040 Vecchi, GA., and A. Wittenberg. (2010): El Niño and our future climate: Where do we stand?
1041 WIREs Clim Change,1, 260–270.
1042
1043 Vincze M., Borcia I. D., Harlander U. (2017) Temperature fluctuations in a changing climate:
1044 an ensemble-based experimental approach. SCIENTIFIC REPORTS. 7: Paper 254. 9 p.
1045
1046 van Vuuren, D. P., J. Edmonds, M. Kainuma, K. Riahi, A. Thomson, K. Hibbard, G. C. Hurtt,
1047 T. Kram, V. Krey, J.-F. Lamarque, T. Masui, M. Meinshausen, N. Nakicenovic, S. J. Smith, S.
1048 K. Rose (2011). The representative concentration pathways: an overview. Climatic Change
1049 109, 5-31.
1050
1051 Walker, G. T., and E. W. Bliss, (1937). World weather VI. Mem. Roy. Meteor. Soc.,4,119–139.
1052

Accepted for publication in *Journal of Climate*. DOI 10.1175/JCLI-D-19-0341.1.

Wilks, D.S. (2016) “The Stippling Shows Statistically Significant Grid Points”: How Research Results are Routinely Overstated and Overinterpreted, and What to Do about It. *Bull. Amer. Meteor. Soc.,* **97**, 2263–2273, https://doi.org/10.1175/BAMS-D-15-00267.1

Wu, R., J. Chen, and W. Chen, 2012: Different Types of ENSO Influences on the Indian Summer Monsoon Variability. J. Climate, 25, 903–920, https://doi.org/10.1175/JCLI-D-11-00039.1

Wunsch, C., 1999: The Interpretation of Short Climate Records, with Comments on the North Atlantic and Southern Oscillations. Bull. Amer. Meteor. Soc., 80, 245–256

Yun, K. S., & Timmermann, A. (2018). Decadal monsoon-ENSO relationships reexamined. Geophys. Res. Lett., 45, 2014–2021. https://doi.org/10.1002/2017GL076912

Zhang T., Sun D.-Z. (2014). ENSO asymmetry in CMIP5 models. J Clim 10(27):4070–4093.

Accepted for publication in *Journal of Climate*. DOI 10.1175/JCLI-D-19-0341.1.

Fig. 1. The nominal radiative forcing Q as a function of time in the particular simulations within the timespan of our investigation. For the nominal radiative forcing in the CESM-LE, the MPI-HE, the MPI-RCP8.5E and in the MPI-RCP2.6E, see Meinshausen et al. (2011). The nominal radiative forcing in the MPI-1pctE has been calculated via the logarithmic response (Ramaswamy et al., 2001).

Fig. 2. The correlation coefficient between the All-India summer monsoon rainfall and Niño 3 (a,c) or SOI (b,d), as a function of the nominal radiative forcing Q (a,b) and time (c,d) in different ensembles as indicated by the coloring (see Fig. 1). For comparability, $-r$ is plotted in panels (a) and (c). For visibility, MPI-RCP2.6E is not included in panels (c) and (d). Consecutive years are connected by lines in all panels.

Fig. 3. The Z_{MK} values (color coded; $|Z_{MK}| > 1.96$ (corresponding to $p_{MK} < 0.05$, shown in Supplementary Fig. S6): red or blue, according to the sign) and slopes calculated in the MPI-HE and MPI-RCP8.5 stitched together for all possible subintervals of the whole time span. ENSO is represented by (a) and (c) Niño 3 and by (b) and (d) SOI.

Fig. 4. Same as Fig. 3 if September is excluded from the monsoon season.

Fig. 5. Same as Fig. 3 for Niño 3.4 and the box-SOI.

Fig. 6. Same as Fig. 3 for the MPI-1pctE. Note the shorter length of the simulation.

Accepted for publication in *Journal of Climate*. DOI 10.1175/JCLI-D-19-0341.1.

Fig. 7. Same as Fig. 3 for the MPI-RCP2.6E stitched after the MPI-HE. Note that the lower triangles are identical to those in Fig. 3.

Fig. 8. Moving temporal correlation coefficient based on observational data (see also the main text). (a) JJAS All-India summer monsoon rainfall data; (b) JJA mean Niño 3 index based on the ERSST v5 dataset. In both of these diagrams a 21-year running mean is shown as well as a smoothing of it obtained by the Savitzky-Golay filter (of order 3 and a window size of 21 years, *applying Matlab's 'sgloayfilt'). This is what is subtracted from the original data, in ways of detrending, following KK99. (c) "Anomalies" obtained following KK99, providing visuals of correlation. (d) The correlations coefficient itself, obtained by both the direct method of YT18 and the method of KK99.*

Fig. 9. Moving temporal correlation coefficient, following YT18, based on various observational variable combinations. Robustness is examined by "perturbing" both the (a) precipitation and (b) SST variables. The legends indicate the following combinations: #1 – (ERSST v5, AISMR); #2 – (ERSST v5, CRU PRE masked with the AISMR regions); #3 – (ERSST v5, CRU PRE in the box [5°N–25°N, 70°E–90°E] (Yun & Timmermann, 2018)); #4 – (ERSST v5, AISMR JJA only); #5 – (HadISST1, AISMR); #6 – (ERSST v4, AISMR); #7 – (ERSST v5 eastern half of Niño 3 box, AISMR).

Fig. 10. Moving temporal correlation coefficient for all converged members of the MPI-GE in the historical period continued seamlessly with the RCP8.5 forcing scenario, following both (a) KK99 and (b) YT18. The thin gray lines show all the realisations while 3 realisations are shown in colour for example. Thick blue lines show the ensemble average of the temporal correlation, which are blown up in insets to better indicate any trend.

Accepted for publication in *Journal of Climate*. DOI 10.1175/JCLI-D-19-0341.1.

Fig. 11. Climatological SST trend in model and observation. (a) Ensemble-mean and (b) standard-deviation of the SST trend in the MPI-HE (1880-2005); (c) SST trend in the ERSST v5 (1880-2016) data set.

Fig. 12. Climatological JJAS mean precipitation in model and observation. (a) Ensemble-mean and (b) standard-deviation of the JJAS mean precipitation in the MPI-HE (1880-2005); (c) JJAS mean precipitation in the CRU PRE (1900-2010) data set (data available only over land).

Fig. 13. Same as Fig. 12 but for long-term temporal trends of JJAS mean precipitation.

Fig. 14. Comparison of large-area-averages in model (MPI-ESM) and observation (precipitation: AISMR magenta; SST: ERSST v5, blue). (a) JJAS precipitation; (b) JJA SST. To match the AISMR data, precipitation in the model is averaged over the AISMR areas (India, except for a few states; see main text). The JJA SST is averaged in the Niño 3 box. Thin gray lines represent all converged members of the MPI-GE, while three coloured lines show examples of individual members; the thick blue lines show the ensemble mean.

Accepted for publication in *Journal of Climate*. DOI 10.1175/JCLI-D-19-0341.1.

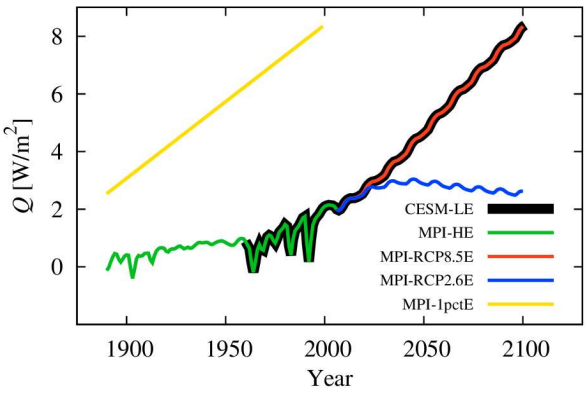

Fig. 1. The nominal radiative forcing Q as a function of time in the particular simulations within the timespan of our investigation. For the nominal radiative forcing in the CESM-LE, the MPI-HE, the MPI-RCP8.5E and in the MPI-RCP2.6E, see Meinshausen et al. (2011). The nominal radiative forcing in the MPI-1pctE has been calculated via the logarithmic response (Ramaswamy et al., 2001).

Accepted for publication in *Journal of Climate*. DOI 10.1175/JCLI-D-19-0341.1.

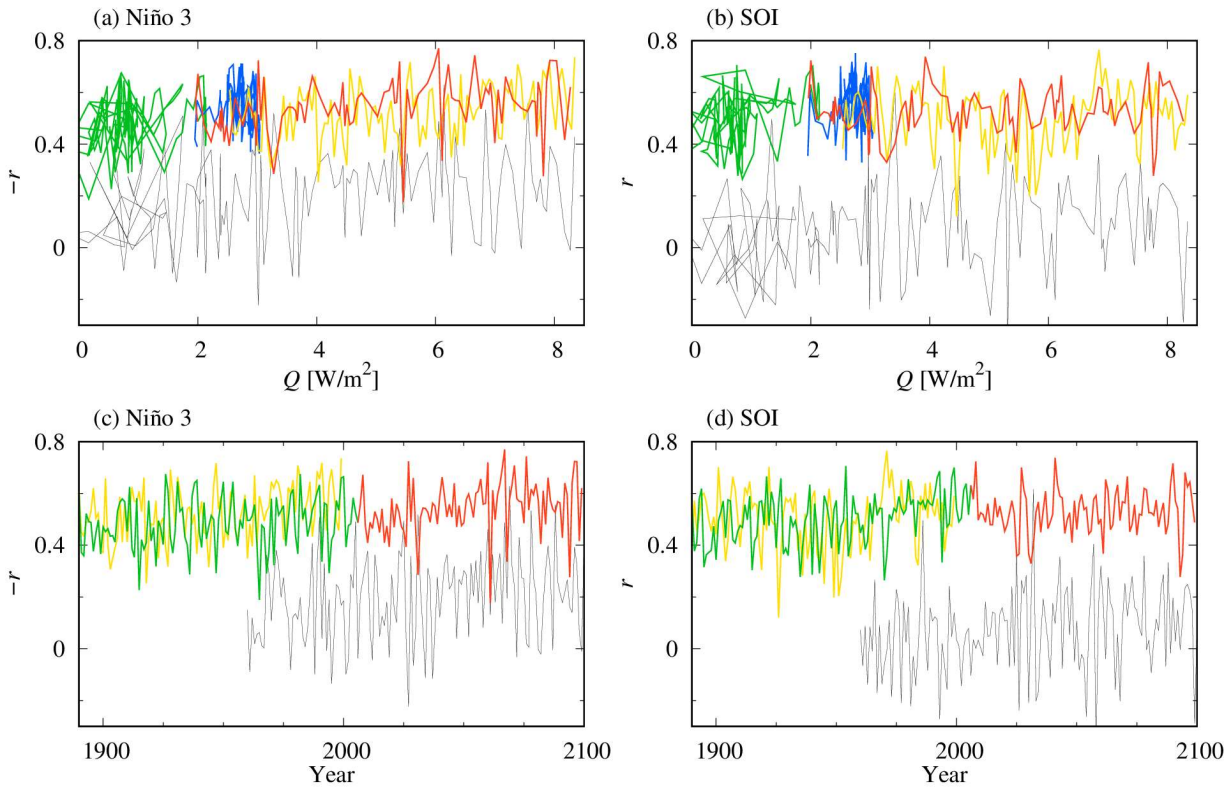

Fig. 2. The correlation coefficient between the All-India summer monsoon rainfall and Niño 3 (a,c) or SOI (b,d), as a function of the nominal radiative forcing Q (a,b) and time (c,d) in different ensembles as indicated by the coloring (see Fig. 1). For comparability, $-r$ is plotted in panels (a) and (c). For visibility, MPI-RCP2.6E is not included in panels (c) and (d). Consecutive years are connected by lines in all panels.

Accepted for publication in *Journal of Climate*. DOI 10.1175/JCLI-D-19-0341.1.

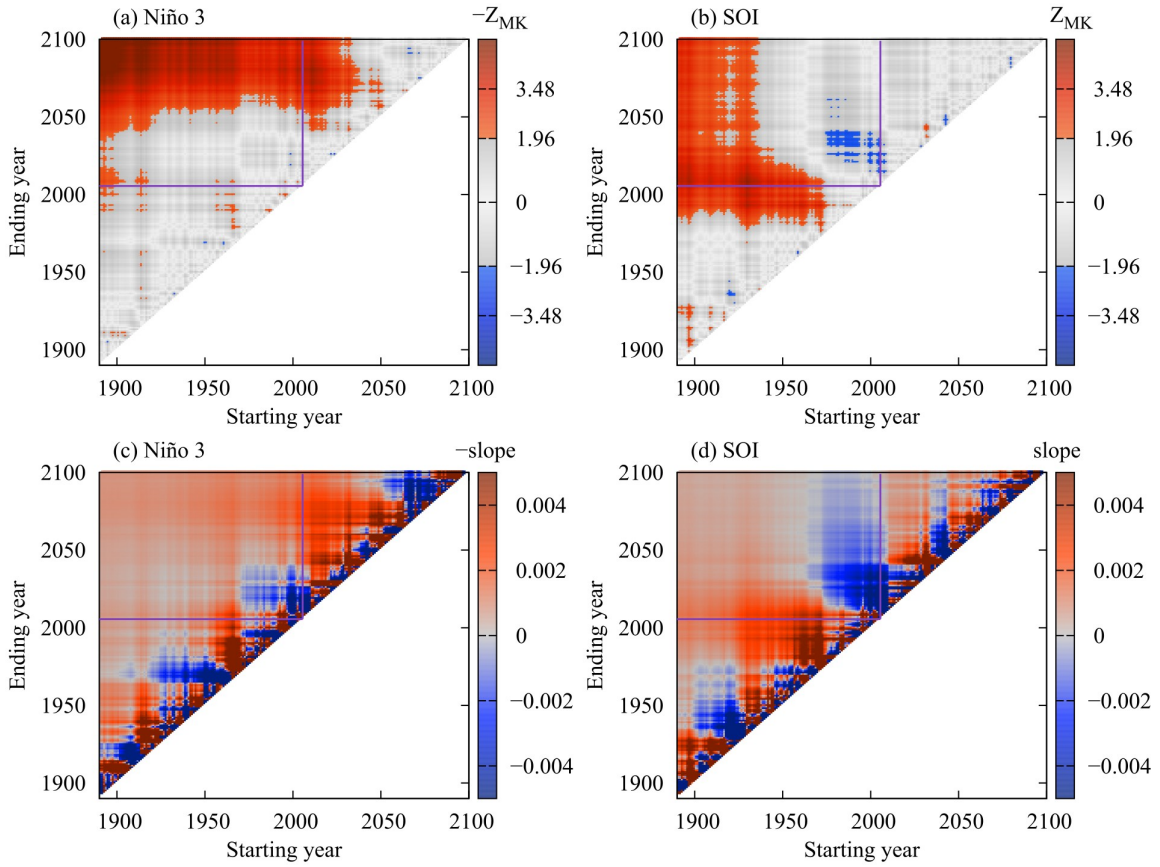

Fig. 3. The Z_{MK} values (color coded; $|Z_{MK}| > 1.96$ (corresponding to $p_{MK} < 0.05$, shown in Supplementary Fig. S6): red or blue, according to the sign) and slopes calculated in the MPI-HE and MPI-RCP8.5 stitched together for all possible subintervals of the whole time span. ENSO is represented by (a) and (c) Niño 3 and by (b) and (d) SOI.

Accepted for publication in *Journal of Climate*. DOI 10.1175/JCLI-D-19-0341.1.

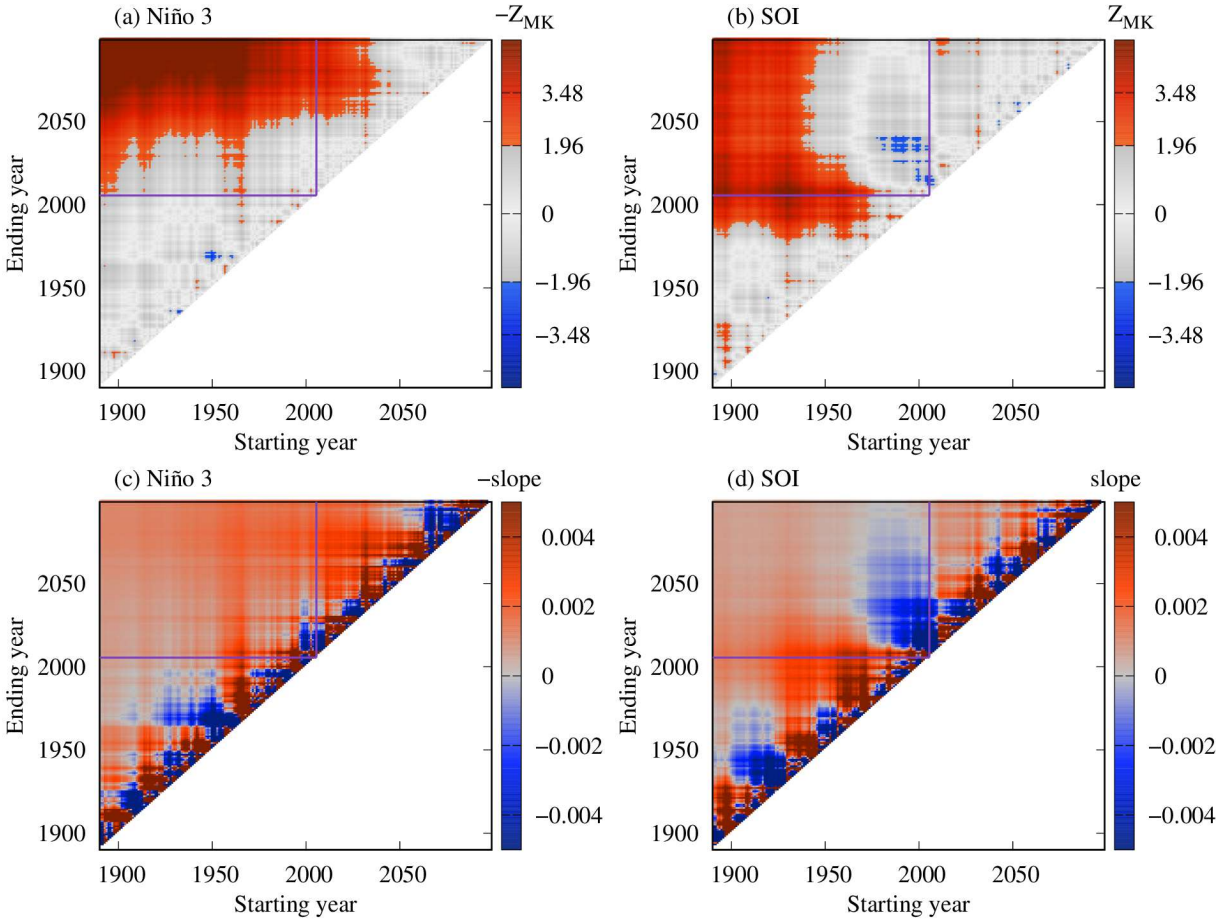

Fig. 4. Same as Fig. 3 if September is excluded from the monsoon season.

Accepted for publication in *Journal of Climate*. DOI 10.1175/JCLI-D-19-0341.1.

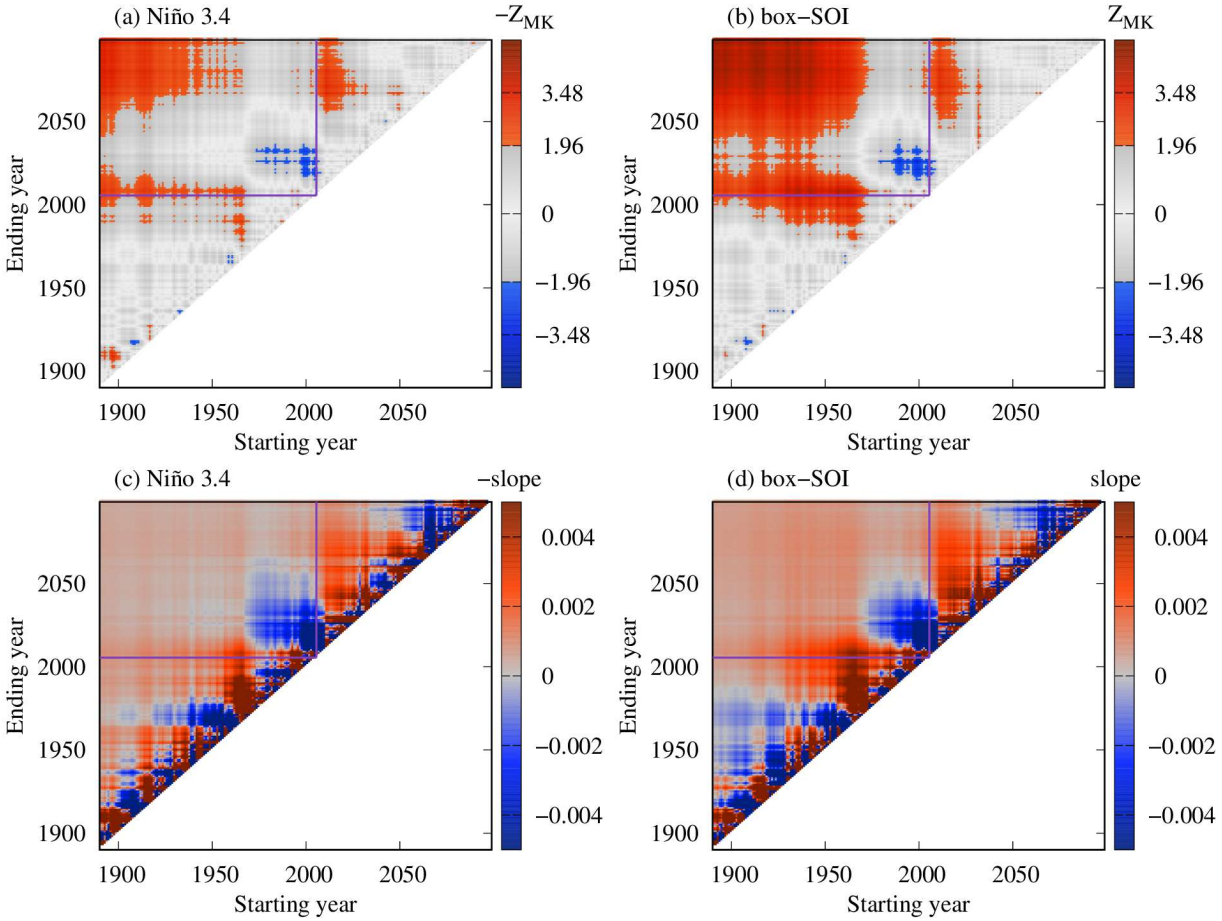

Fig. 5. Same as Fig. 3 for Niño 3.4 and the box-SOI.

Accepted for publication in *Journal of Climate*. DOI 10.1175/JCLI-D-19-0341.1.

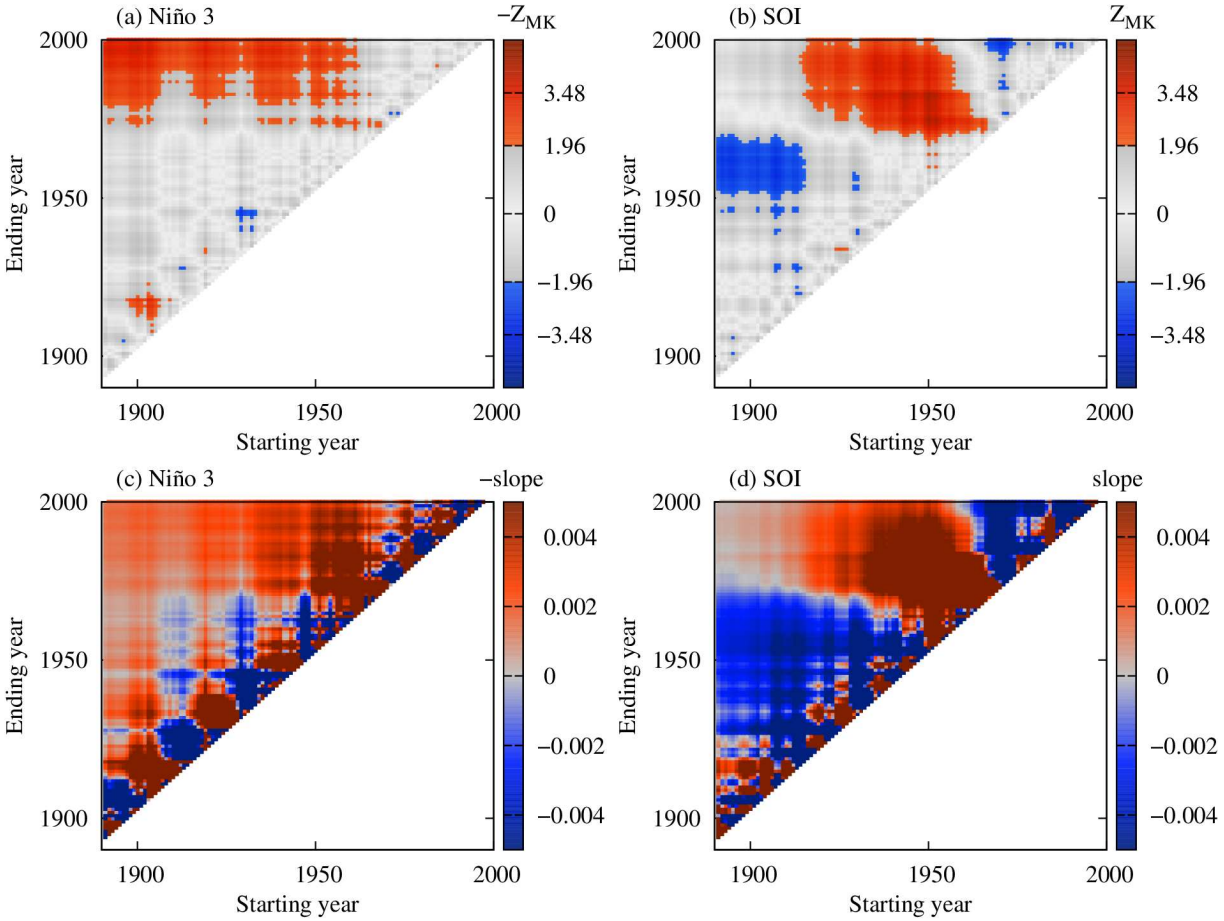

Fig. 6. Same as Fig. 3 for the MPI-1pctE. Note the shorter length of the simulation.

Accepted for publication in *Journal of Climate*. DOI 10.1175/JCLI-D-19-0341.1.

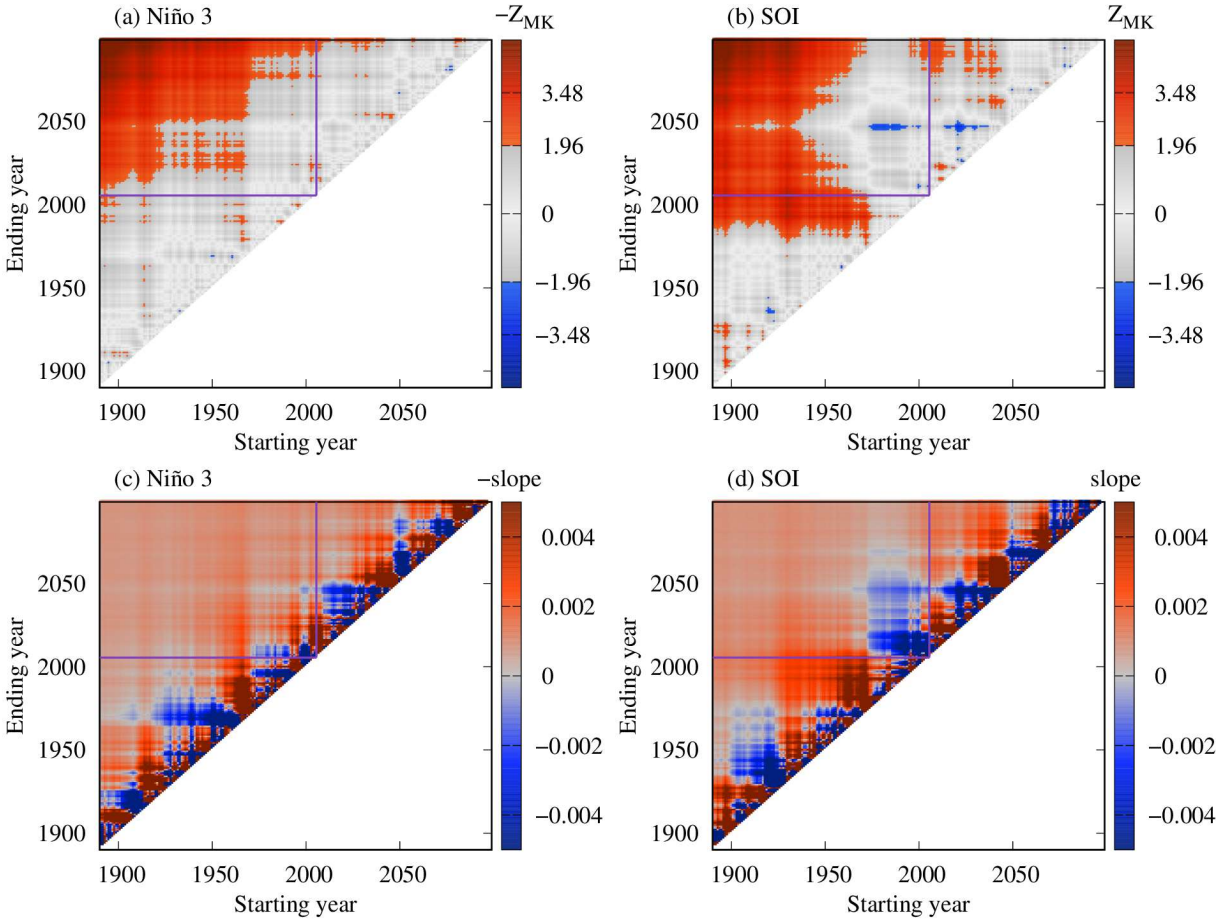

Fig. 7. Same as Fig. 3 for the MPI-RCP2.6E stitched after the MPI-HE. Note that the lower triangles are identical to those in Fig. 3.

Accepted for publication in *Journal of Climate*. DOI 10.1175/JCLI-D-19-0341.1.

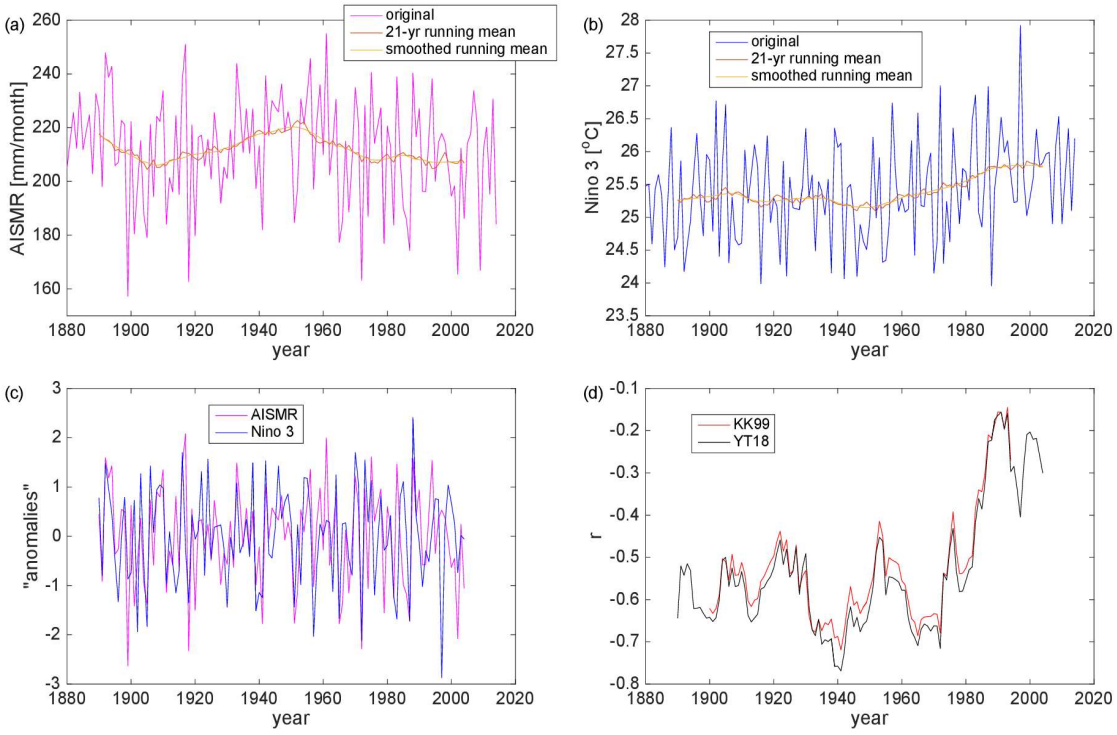

Fig. 8. Moving temporal correlation coefficient based on observational data (see also the main text). (a) JJAS All-India summer monsoon rainfall data; (b) JJA mean Niño 3 index based on the ERSST v5 dataset. In both of these diagrams a 21-year running mean is shown as well as a smoothing of it obtained by the Savitzky-Golay filter (of order 3 and a window size of 21 years, *applying Matlab's 'sgloayfilt'). This is what is subtracted from the original data, in ways of detrending, following KK99. (c) "Anomalies" obtained following KK99, providing visuals of correlation. (d) The correlations coefficient itself, obtained by both the direct method of YT18 and the method of KK99.*

Accepted for publication in *Journal of Climate*. DOI 10.1175/JCLI-D-19-0341.1.

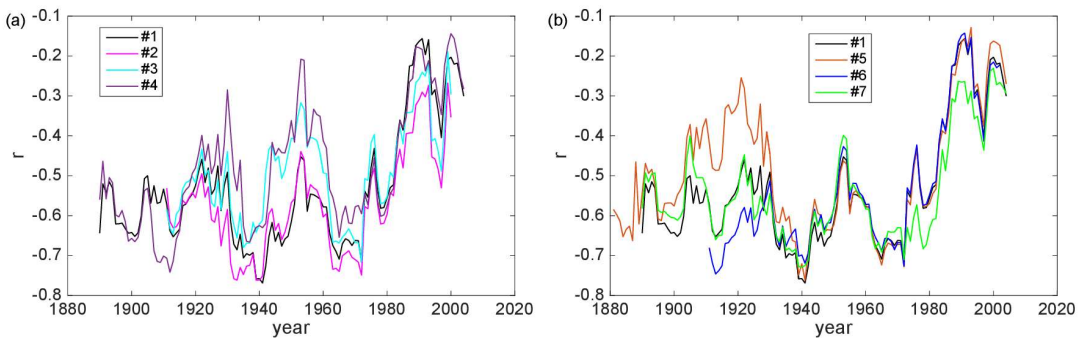

Fig. 9. Moving temporal correlation coefficient, following YT18, based on various observational variable combinations. Robustness is examined by "perturbing" both the (a) precipitation and (b) SST variables. The legends indicate the following combinations: #1 – (ERSST v5, AISMR); #2 – (ERSST v5, CRU PRE masked with the AISMR regions); #3 – (ERSST v5, CRU PRE in the box [5°N–25°N, 70°E–90°E] (Yun & Timmermann, 2018)); #4 – (ERSST v5, AISMR JJA only); #5 – (HadISST1, AISMR); #6 – (ERSST v4, AISMR); #7 – (ERSST v5 eastern half of Niño 3 box, AISMR).

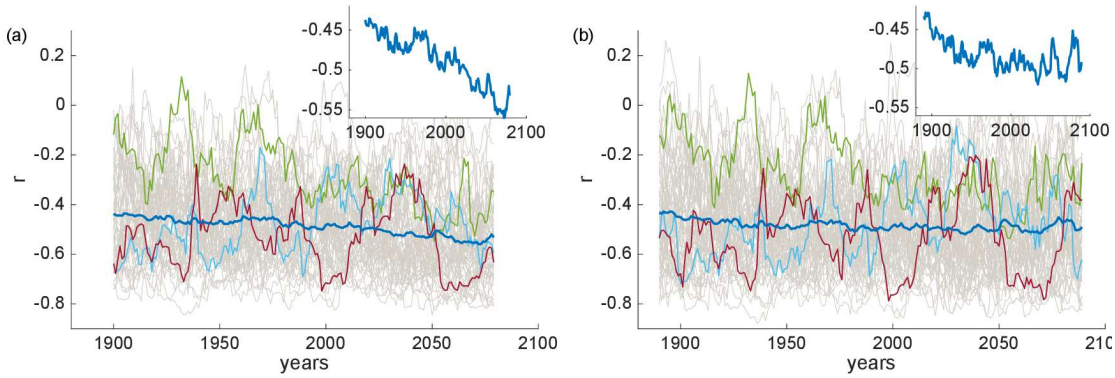

Fig. 10. Moving temporal correlation coefficient for all converged members of the MPI-GE in the historical period continued seamlessly with the RCP8.5 forcing scenario, following both (a) KK99 and (b) YT18. The thin gray lines show all the realisations while 3 realisations are shown in colour for example. Thick blue lines show the ensemble average of the temporal correlation, which are blown up in insets to better indicate any trend.

Accepted for publication in *Journal of Climate*. DOI 10.1175/JCLI-D-19-0341.1.

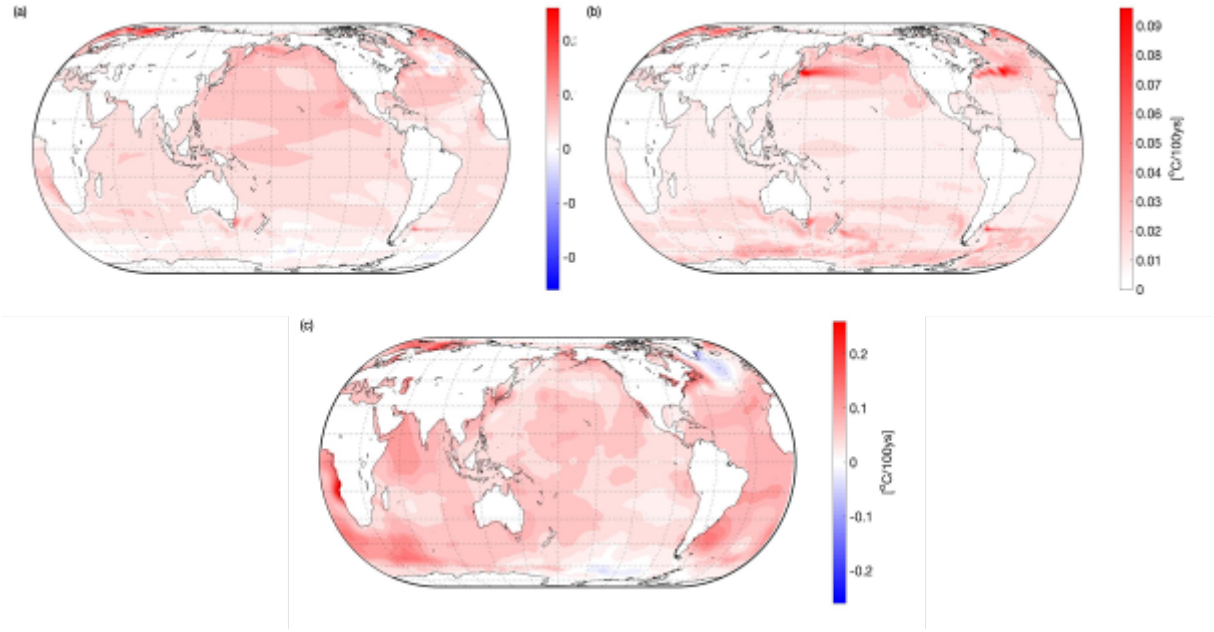

Fig. 11. Climatological SST trend in model and observation. (a) Ensemble-mean and (b) standard-deviation of the SST trend in the MPI-HE (1880-2005); (c) SST trend in the ERSST v5 (1880-2016) data set.

Accepted for publication in *Journal of Climate*. DOI 10.1175/JCLI-D-19-0341.1.

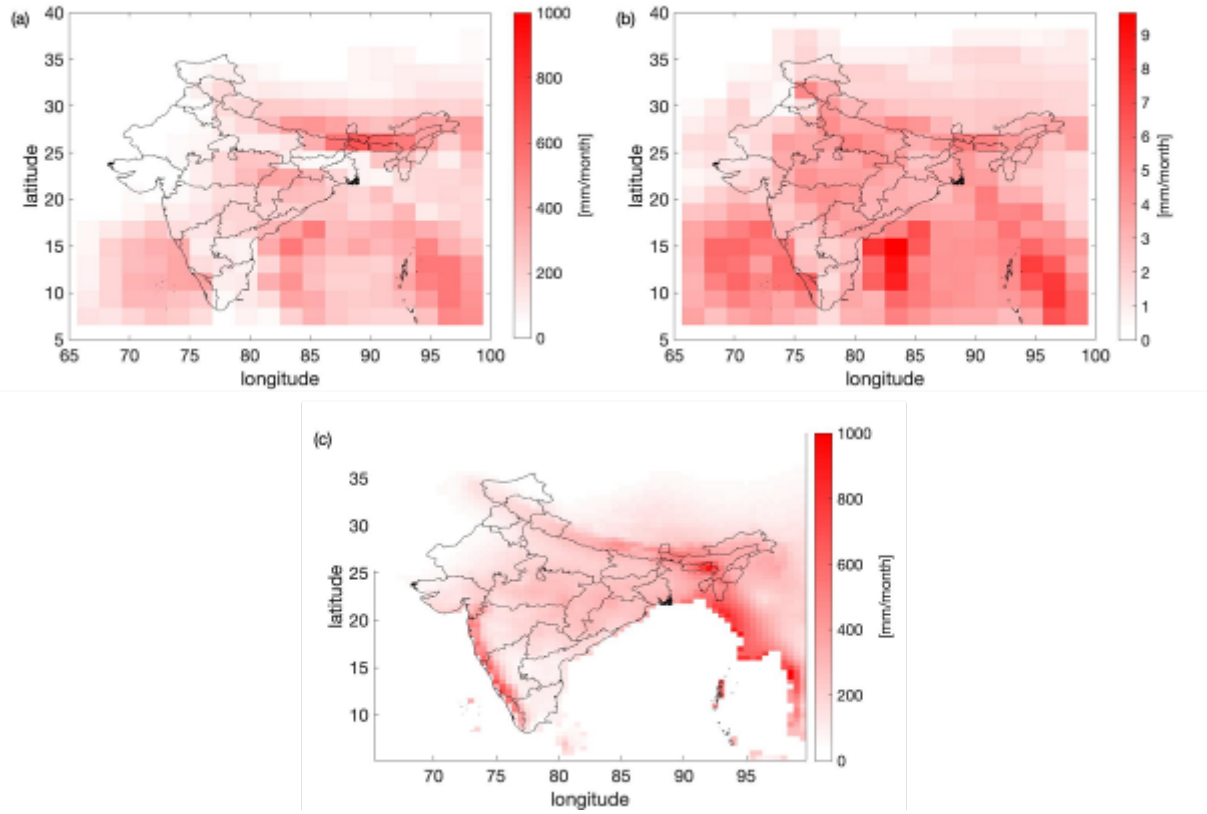

Fig. 12. Climatological JJAS mean precipitation in model and observation. (a) Ensemble-mean and (b) standard-deviation of the JJAS mean precipitation in the MPI-HE (1880-2005); (c) JJAS mean precipitation in the CRU PRE (1900-2010) data set (data available only over land).

Accepted for publication in *Journal of Climate*. DOI 10.1175/JCLI-D-19-0341.1.

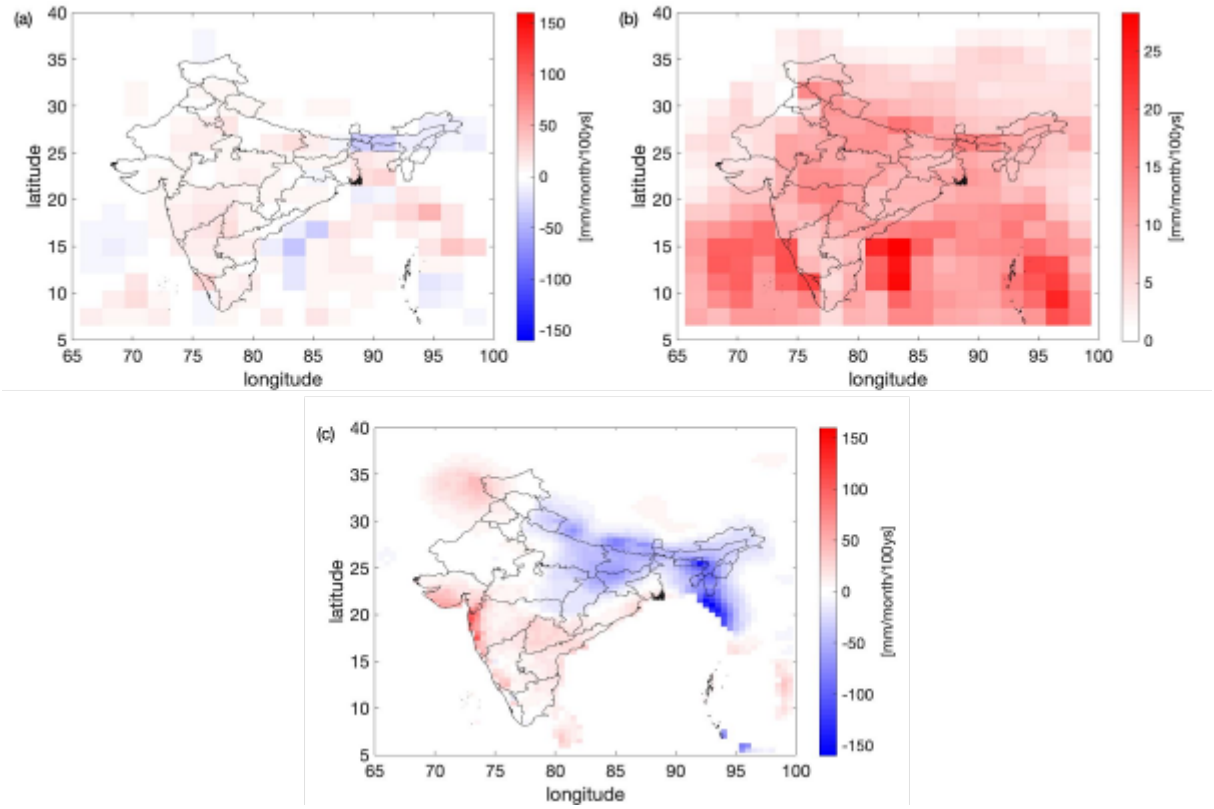

Fig. 13. Same as Fig. 12 but for long-term temporal trends of JJAS mean precipitation.

Accepted for publication in *Journal of Climate*. DOI 10.1175/JCLI-D-19-0341.1.

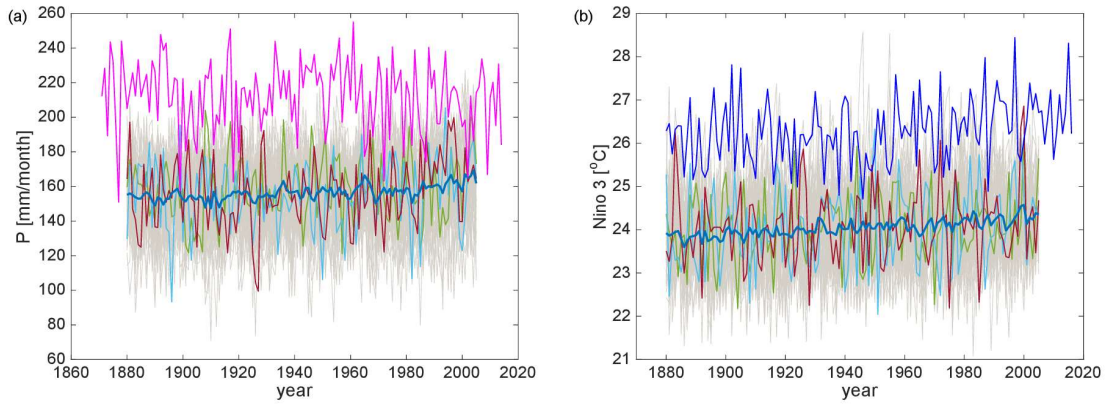

Fig. 14. Comparison of large-area-averages in model (MPI-ESM) and observation (precipitation: AISMR magenta; SST: ERSST v5, blue). (a) JJAS precipitation; (b) JJA SST. To match the AISMR data, precipitation in the model is averaged over the AISMR areas (India, except for a few states; see main text). The JJA SST is averaged in the Niño 3 box. Thin gray lines represent all converged members of the MPI-GE, while three coloured lines show examples of individual members; the thick blue lines show the ensemble mean.

Accepted for publication in *Journal of Climate*. DOI 10.1175/JCLI-D-19-0341.1.